学位申請論文

下林典正

主 論 文

High Temperature Transmission Electron Microscopy of the Polymorphic Phase Transformation in Ca-poor Pyroxenes

by

Norimasa SHIMOBAYASHI

December, 1989

Doctoral Thesis,
Department of Geology and Mineralogy,
Faculty of Science, Kyoto University

Abstract

A new heating stage for high temperature transmission electron microscopy (HTTEM) was constructed for *in situ* observations up to 1300°C. In this study, the changes in both the textures and structures of Ca-poor pyroxenes (enstatite and pigeonite) during the polymorphic phase transformations were *in situ* observed successfully for the first time using the HTTEM system.

Both orthoenstatite and clinoenstatite transformed to high-clinoenstatite, not to protoenstatite of a stable phase at high temperatures. The phase transformation from orthoenstatite to high-clinoenstatite was first reported in this study.

The high($C2/c$)-low($P2_1/c$) phase transformations in clinoenstatite and pigeonite were also observed *in situ* at high temperatures under the HTTEM. The coexistence of both high-low phases with the coherent interfaces and the time-independent reactions suggested that the $P2_1/c$-$C2/c$ phase transformation is of a first-order and occurs martensitically From the unusual thermal hysteresis, the $P2_1/c$-$C2/c$ phase transformation was revealed to be a thermoelastic type of the martensitic transformation. This type of the phase transformation had not been reported in rock-forming minerals

The formation process of the antiphase boundaries (APB's) in pigeonite was also *in situ* observed during the

phase transformation using the HTTEM. It is illustrated that the APB's parallel to the *c* axis form at the earlier stage and the APB's cutting the *c* axis form at the final stage of the $C2/c$-to-$P2_1/c$ phase transformation on cooling. These observations gave a reasonable explanation to the fact that the former type of APB's is commonly observed in the rapidly cooled pigeonite while the latter type of APB's tends to be in majority in the slowly cooled pigeonite.

Contents

Introduction

Phase transformations of minerals have been studied extensively to elucidate the mineral behaviours during the mineral formation. Pyroxene is one of the most important rock-forming minerals not only for its abundant occurrence but also for its various microtextures, which provide an information on the thermal or stress history of the rocks containing it. Any pyroxene belongs to either the monoclinic or orthorhombic crystal system. The common rock-forming pyroxenes belong to the pyroxene quadrilateral of the $Mg_2Si_2O_6$(En) - $Fe_2Si_2O_6$(Fs) - $CaMgSi_2O_6$(Di) - $CaFeSi_2O_6$(Hd) system. Four different structural types have been known in this quadrilateral at the atmospheric pressure.

Phase relations of four polymorphs in the quadrilateral

Monoclinic pyroxenes (clinopyroxenes) in this pyroxene quadrilateral have a wide range of chemical composition and are classified into two groups: Ca-rich one (space group: $C2/c$) and Ca-poor one (space group: $P2_1/c$) On heating, the Ca-poor $P2_1/c$ clinopyroxene undergoes a rapid displacive transformation to the $C2/c$ structure, which cannot be quenched. This $C2/c$ phase of the Ca-poor part is isostructural with the Ca-rich one, but there are a miscibility gap between them. On the other hand, the Ca-

rich clinopyroxene does not show this type of transformation.

Orthopyroxene (space group: *Pbca*) occurs in a limited composition range from $Mg_2Si_2O_6$ to $Fe_2Si_2O_6$ with only less than 5 mole percent of the $Ca_2Si_2O_6$ (Wo) component. Protoenstatite (space group: *Pbcn*), the other orthorhombic form, exists only at the enstatite corner of the quadrilateral (protoenstatite), which is stable only at high temperatures.

Smith (1969a) has summarized lots of the stability data of enstatite and concluded that orthoenstatite is the stable phase at low temperatures. On the contrary, Grover (1972) suggested that clinoenstatite ($P2_1/c$) is the stable phase because of his success in crystallizing it below 566°C using a flux method. However, clinoenstatite is thought to be not stable under the hydrostatic pressure conditions as pointed out by Ozima (1982), who synthesized orthoenstatite using a flux method. Thus most subsequent authors have tended to agree that orthopyroxene is the stable phase rather than clinopyroxene ($P2_1/c$)

Phase transformation among four polymorphs

The polymorphic phase transformations occur only in the Ca-poor part of the quadrilateral. Therefore, the present study will be focussed upon the phase transformations in the Ca-poor pyroxenes Hereafter, above four polymorphic phases of the Ca-poor pyroxenes are denoted as *ortho*, *proto*,

clino(P), and *clino(C)*, respectively

(a) Phase transformations associated with *proto*

Proto is stable only at high temperatures and cannot be quenched. On cooling, *proto* transforms to either *ortho* or *clino(P)*.

The *ortho*-to-*proto* transformation of enstatite was extensively studied using a high temperature X-ray single crystal method by many investigators as summarized by Smith (1969a) Smyth (1974a) studied in detail on the phase transformations among *ortho*, *proto* and *clino(P)* using the high temperature X-ray single crystal method, but did not observe any transformation to *clino(C)*. Then, he found that the phase transformation between *clino(P)* and *proto* is essentially instantaneous, diffusionless, oriented, reversible and time-independent, and thus concluded that this phase transformation occurs martensitically. The *clino(P)*-to-*proto* phase transformation was also reported by Sadanaga *et al.* (1969), whereas they indicated two courses of the transformation to *proto*: one *via* 'ortho-like phase', and the other *via clino(C)*. The former path can be considered to be the phase transformation from metastable *clino(P)* to stable *ortho* by annealing, as reported by Smyth (1974a) and Coe and Kirby (1975) However, the latter path shows the possibility of the *clino(P)*-to-*clino(C)* phase transformation even in enstatite, as well as in clinohypersthene and clinoferrosilite. Sadanaga and Okamura

(1971) reexamined the latter path and comfirmed it by structure analysis. There remains still in controversy in the kinetics of the phase transformations related with *proto*.

(b) Phase transformation between *ortho* and *clino(P)*

The *ortho*-to-*clino(P)* phase transformation has been known as a stress-induced transformation, not a temperature-induced one. Turner *et al.* (1960) first showed experimentally that mechanical deformation can induce the transformation suggesting a martensitic reaction with slip on (100) Kirby and Coe (1974) reported that a shape change of a enstatite crystal occurs during the transformation, confirming its martensitic nature.

The reverse phase transformation, *clino(P)*-to-*ortho*, was reported by Smyth (1974a) and Coe and Kirby (1975).

(c) Phase transformation between *ortho* and *clino(C)*

The *ortho*-to-*clino(C)* phase transformation has not been reported for enstatite, owing to the existence of *proto* as a stable high temperature phase However, this type of phase transformation were well-known for hypersthene (Smyth, 1969) and ferrosilite (Sueno and Prewitt, 1983)

Clino(C) is an unquenchable phase. During very slow cooling, *clino(C)* must transform reconstructively to *ortho* or *ortho* with an exsolution of augite However, this type of phase transformation has not been experimentally

confirmed, because the sluggishness of the reaction has precluded definitive experiments. On rapid cooling, however, a displacive transformation occurs and *clino(C)* transforms to metastable *clino(P)*

(d) Phase transformation between *clino(P)* and *clino(C)*

The phase transformation between *clino(P)* and *clino(C)* (hereafter simply *P-C* phase transformation) is reversible. Because *clino(C)* is an unquenchable phase, the *P-C* phase transformation has been studied by heating experiments.

The *P-C* phase transformation was suggested by Morimoto and Tokonami (1969) for pigeonite and was first reported by Smith (1969b) after reinterpreting data from Perrotta and Stephenson (1965) for clinoenstatite. The phase transformation has been observed experimentally using high temperature single crystal X-ray techniques by Smyth (1969, 1974b) for clinohypersthene, by Prewitt *et al.* (1970) and Prewitt *et al.* (1971) for pigeonite, by Sadanaga and Okamura (1971) for clinoenstatite, and by Sueno and Prewitt (1983) for clinoferrosilite. The temperature of the *P-C* phase transformation of Ca-poor clinopyroxenes depends on their compositions, ranging from above 1000°C for Mg-rich ones to 500°C for Fe-rich ones (Prewitt *et al.*, 1971)

Antiphase domain (APD) structure is a typical resulting microstructure of the *clino(C)*-to-*clino(P)* phase transformation. Especially, the APD structure in pigeonite is closely related to the cooling rate Many attempts

have been made to use the size of APD's in pigeonite as a relative cooling ratemeter (*e.g.* Ghose *et al* , 1972; Lally *et al.*, 1975; Grove, 1979; Carpenter, 1979) Recently, Fujino *et al.* (1988) suggested that the orientation of antiphase boundaries (APB's), rather than the size of APD's, would be closely associated with the cooling rate.

Among above polymorphic phase transformations in the Ca-Mg-Fe pyroxenes, the study of the *P-C* phase transformation has been comparatively progressed for its importance as an information on the thermal histories.

Smyth (1974b) suggested that the *P-C* phase transformation was thermodynamically of a first-order because of a discontinuous change in unit cell dimensions, based on the study using the high temperature X-ray single crystal method for clinohypersthene However, the possibility that it is of a second or higher order has not been completely ruled out. For example, Buseck *et al.* (1980) treated the *P-C* phase transformation in pigeonite as a second-order transformation for the discussion of exsolution in pyroxenes (as shown in their Figure 9) Although there are a number of the experimental works of the *P-C* phase transformation, the nature of the transformation is not well understood.

As for the APD structures in pigeonites, furthermore, all of the works were carried out using the natural

specimens or the quenched products of the annealing experiments although *clino(C)* is unquenchable. No direct imaging for the formation process of APD structure in pigeonite has been *in situ* observed at high temperatures.

Therefore, the *in situ* observation at high temperatures is indispensable for the study on the polymorphic phase transformations of pyroxenes, because some important phases are unquenchable. The *in situ* experiments at high temperatures were employed only by use of the high temperature X-ray method. On the other hand, transmission electron microscopy (TEM) is one of the most effective techniques to study the phase transformation, because observations of the fine textures of minerals bring out various characteristics of the phase transformation. The *in situ* observation of transformation at high temperatures under the TEM was also expected to give much information on mineral behaviours during the phase transformation. However, a technical difficulty for keeping the specimens at high temperatures in the TEM has retarded the development of high temperature transmission electron microscopy (HTTEM) Preliminary work on HTTEM of pigeonite has been carried out by Feuer *et al* (1986), whereas they could not reveal the nature of the phase transformation of pigeonite because they used a single-tilting stage.

In the present study, a new double-tilting heating stage was constructed for the *in situ* observation above 1200°C under the TEM (Morimoto *et al* , 1989) This HTTEM

system was employed to study the polymorphic phase transformation of Ca-poor pyroxene, especially to elucidate the nature of the *P-C* phase transformation. As the result, the present HTTEM system has been proved to be effective to the studies on the phase transformations in pyroxenes, although the vaporization of some specimens is inevitable under such a high temperature and high vacuum conditions.

In the present HTTEM studies, *ortho*-to-*clino(C)* phase transformation in enstatite was first observed and new information on the *P-C* phase transformations are obtained. The *P-C* phase transformations of clinoenstatite and pigeonite are revealed to occur athermal martensitically and even thermoelastically (see Appendix) This thermoelastic martensitic transformation has not been reported in rock-forming minerals. Accompanied with the *P-C* phase transformation, the formation process of the APD structure was also discussed.

2. High Temperature Transmission Electron Microscopy

2.1 Previous heating stages

Heating apparatuses for the HTTEM have been designed in various styles and are put on the market as an optional part. According to Tighe (1976), two types of heaters have been used: (a) a strip heater with a grid of holes, and (b) a non-inductively wound furnace. The furnaces can have a more uniform temperature distribution than the strip heaters although the strip heaters can be achieved much higher temperatures , *e.g.* up to about 3000°C (McPartland, 1962), than the furnaces. However, the usage of the heating stages using the furnaces have been usually limited below 1000°C (*e.g.*, Valde, 1972; Henderson-Brown *et al.*, 1972) The heating stage with a furnace available up to 1300°C (Gatan, Model 628) is rather exceptional and made with a single-tilting stage.

Top-entry heating stages are difficult to design because the tilting mechanisms are quite complex. On the other hand, side-entry heating stages have originally one tilt axis and both the power and thermocouple leads can be easily attached to the heater Therefore, the side-entry stages with a furnace are commonly used for the HTTEM.

Special crystal orientations of a specimen are required for the study of fine textures during the phase transformation. However, the required orientations are very changeable at high temperature experiments, and it is almost

impossible to adjust the required orientations by a single-tiling stage Thus, the *in situ* observation of the phase transformations of silicate minerals using the HTTEM with a single-tilting stage has not been succeeded at over 1000°C. Therefore, a double-tilting stage with tilting devices in both the X- and Y-axes of the TEM is indispensable for the HTTEM study of silicate minerals, which are generally of low symmetry classes.

2.2 Construction of a new heating stage

A new heating stage for the HTTEM has been constructed for a 200 kV TEM (HITACHI-H700H) by taking the following points into consideration.

(1) Observation at temperatures up to about 1300°C is possible because many changes in microstructures of important rock-forming minerals are expected to occur only at such high temperatures.

(2) A double-tilting stage can be used at such high temperatures because many rock-forming minerals have such complex structures that Bragg conditions for electron diffraction can be rarely obtained without the double-tilting stage.

(3) Temperatures of specimens can be measured as accurate as possible because the temperature is the most important factor for studying phase transformations under the HTTEM.

A cross section of the new heating stage is shown in Figure 1 A double-tilting side-entry stage is used with the new special furnace at its head part A foil specimen is held between two single-hole meshes of molybdenum and fixed with a carbon screw in the furnace. The heater of the furnace is resistance coils (3 3 mm in diameter and 2 mm in height) embedded in the alumina insulator A tungsten wire (0.15 mm in diameter) is used for the coils (a resistance of 2 Ω at the room temperature) The coils are doubly and reversely wound to suppress the magnetic field generated by

the current applied to the coil heater.

The temperature is controlled by the wattage of the coil heater. The maximum voltage and current are about 10 V and 1 1 A, respectively. To monitor the temperature, the $Pt_{13}Rd$-Pt thermocouple is placed near the outer wall of the furnace. The furnace attached with the thermocouple can be tilted in the Y-axis by pulling a tantalum ribbon wound on the furnace.

The furnace is surrounded by threefold thermal shields of tantalum platelets. The outer shield is attached to a cold finger of the TEM. The inner shield attached to the furnace is twofold. Owing to the small specimen supporter (2.0 mm in diameter), enough space for the inner shield was obtained. This thermal shield alignment (totally threefold) was successful in obtaining the temperature up to about 1300°C. By the use of the inner shield the thermocouple must be placed rather far from a specimen, and the tilt angles are restricted within 10 degrees in the X- and Y-axes of the TEM.

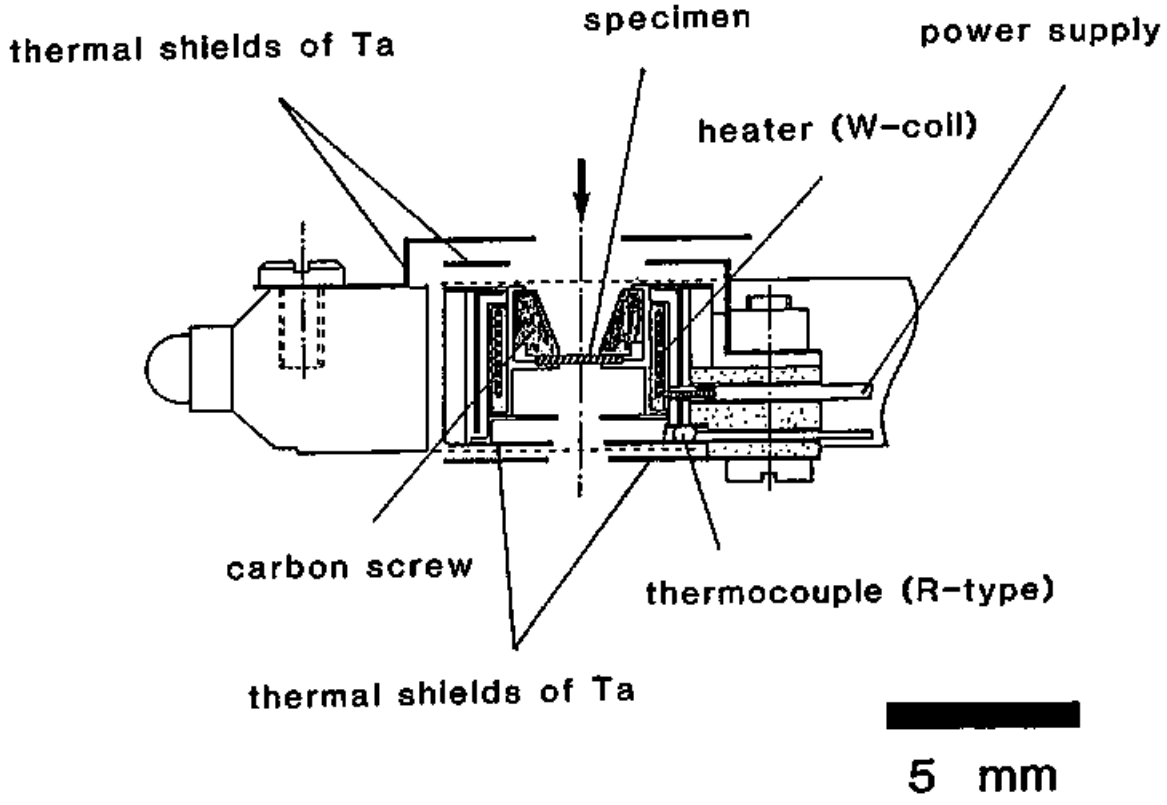

Figure 1. Cross section of a double-tilting side-entry heating stage, newly constructed for a high temperature transmission electron microscope (HTTEM). An arrow indicates the direction of the incident electron beam.

2.3 Temperature calibration

Because temperatures of the small region observed under the HTTEM cannot be measured directly by a thermocouple, the temperatures were estimated by the following way

The heating stage without a specimen was set in a vacuum chamber, and a $Pt_{13}Rd$-Pt thermocouple was placed at the specimen position tentatively in addition to the thermocouple at its own position on the outer wall of the furnace. Two kinds of temperatures were measured using these two thermocouples by changing the wattage applied to the heater These temperatures were plotted against the wattage (Figure 2) The temperature up to about 1300°C was attained at the specimen position in the vacuum chamber. After the preliminary experiments in the vacuum chamber, the heating stage was set in the TEM. The temperature measured at the thermocouple position in the TEM is almost the same as that in the vacuum chamber at the same wattage This suggests that the specimen temperature in the HTTEM is also the same as in the vacuum chamber.

The calibration curve in Figure 2 was further checked by the *in situ* observation of the high(β)-low(α) phase transformation of quartz at 573°C. A single crystal of low(α)-quartz which was synthesized hydrothermally below the transformation temperature was ion-thinned. An incommensurate phase (γ-phase), which is stable within 2°C around 573°C (*e.g.* Dolino, 1986, for a review), was observed

during the phase transformation between the high(β)- and low(α)-quartz in both the heating and cooling processes. The wattage of the heater at which the γ-phase appeared gave almost the constant specimen temperature of around 573°C estimated from the calibration curve (an asterisk in Figure 2) Several heating and cooling experiments showed that the accuracy of the specimen temperature was within 20°C at 573°C. The concordance of the calibrated specimen temperature in the vacuum chamber with the transformation temperature of quartz in the TEM confirms that the calibration curve is reasonable Hereafter, all of the specimen temperatures in the following HTTEM experiments will be derived from this calibration curve.

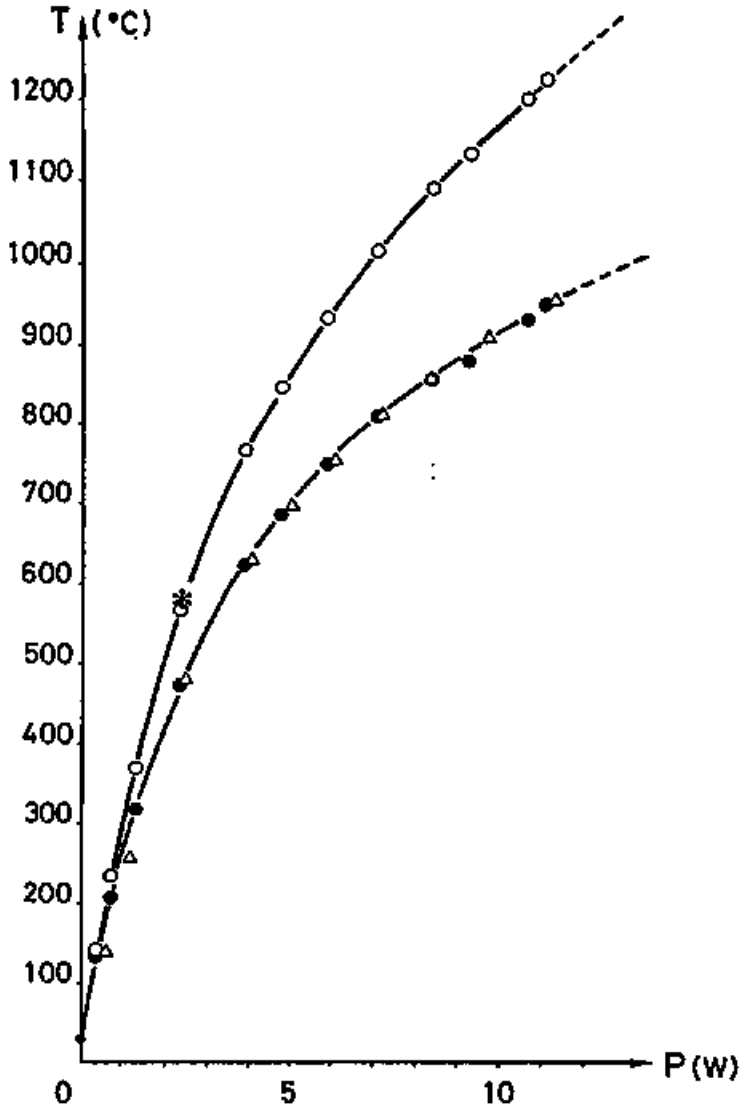

Figure 2. Temperatures at the specimen position (open circles) and at the thermocouple position (solid circles and triangles) plotted against the wattage (P) applied to the heater. The temperatures were measured in a vacuum chamber (open and solid circles) and in the HTTEM (open triangles). A datum point using the $\alpha - \beta$ phase transformation of quartz (573°C) is also shown by an asterisk.

2.4 Pressure and redox conditions

The chamber in the HTTEM is evacuated by a diffusion pump at about $1x10^{-6}$ Torr for generation of an electron beam. The pressure at the specimen position under the HTTEM seems to be the same as the pressure of the chamber or slightly higher due to the degassing by heating from a specimen and a glue (mesh cement) for holding the specimen.

Under a high vacuum condition in the chamber of the HTTEM, specimens usually evaporate from their edges at high temperatures. For example, synthetic enstatite crystals were easily volatilized from their edges, and olivine patches were sometimes formed by incongruent evaporation of the meteoritic enstatite, as described latter.

A reduced condition prevails in the chamber judging from high vacuum and possible contamination of hydrogen carbides from diffusion pump oil. In fact, laihunite, olivine-type mineral with the chemical composition $Fe^{2+}{}_5Fe^{3+}SiO_4$, changed to olivine $Fe^{2+}{}_2SiO_4$ by reduction upon heating in the HTTEM, and never changed back to laihunite again by cooling

2.5 Recording systems of HTTEM

Changes of microstructure of minerals during the phase transformation often occur so rapidly that it is very difficult to take an instantaneous photograph at the moments of the changes. To record such instantaneous changes, a fiber optically coupled TV system (GATAN Model 622) is attached to the HTTEM (Figure 3) A thin yttrium aluminum garnet (YAG) disc (usable area 13 mm x 10 mm), coated with aluminum, is used as the primary screen. It is fiber optically coupled to a TV camera tube with a cadmium zinc telluride target having high resolution and sensitivity plus extreme resistance to blooming and photocathode damage. The image intensifier is mounted between the primary YAG screen and the TV camera target. The control unit with power supply allows manual and auto-control of TV gain and black level, setting of intensifier gain and frequency filtering. Detailed microstructures can be observed on a TV monitor, and these images can be recorded on video tapes. The total system of the present apparatus is schematically shown in a block diagram (Figure 3) Owing to the introduction of this recording system, the thermal drift of the stage (a factor of 100 Å/sec in the extreme case at 1000°C) has not seriously affected the HTTEM observation.

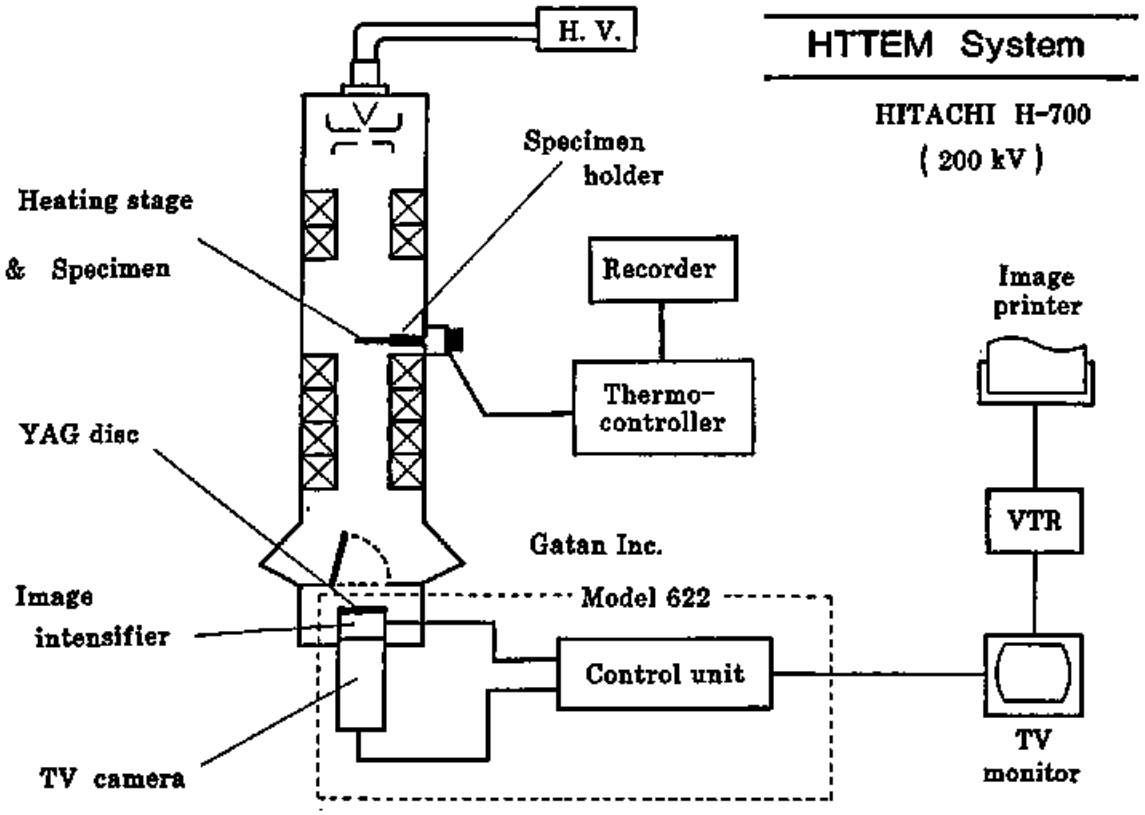

Figure 3. Block diagram of the HTTEM total system. A fiber optically coupled TV system (GATAN 622) is attached to the HTTEM for the record of the instantaneous changes in structures or textures during the HTTEM studies.

3. Experimental

3.1 Specimen preparations

In the present study, the following five kinds of specimens (single crystals) were prepared for the HTTEM observation;

(a) synthetic orthoenstatite (En_{100}): single crystals, produced by a flux method by Ozima (1982);

(b) natural orthoenstatite ($En_{98}Wo_1$): single crystals from the Norton County, Kansas, enstatite achondrite (Reid and Cohen, 1967);

(c) synthetic clinoenstatite (En_{100}): single crystals prepared by heating flux-grown enstatite crystals (Ozima, 1982) at about 1400°C for a week and subsequent rapid quenching;

(d) clinoenstatite ($En_{91}Fs_8Wo_1$): phenocrysts in boninite from Muko-Jima, the Bonin Islands, Japan (Komatsu, 1980; Shiraki *et al* , 1980);

(e) pigeonite ($En_{58}Fs_{39}Wo_3$): phenocrysts with minor augite ($En_{42}Fs_{23}Wo_{35}$) lamellae in andesite from Hakone-toge, Hakone Volcano, Japan (Kuno, 1936)

The chemical compositions of the specimens were determined with either EPMA (Hitachi S-530) or analytical-TEM (ATEM: Hitachi H-700; Morimoto and Kitamura, 1981), both of which are equipped with a *Kevex* EDS (DELTA Class) system.

Each specimen was cut into (010) section and polished mechanically until about 30 μm thick. Then specimens were mounted on 2 mmø molybdenum single-hole meshes (0 1 mmø hole diameter), thinned by ion bombardment, and carbon-coated on both sides to improve electrical conductivity

In the heating experiments, temperatures were raised or lowered usually stepwise by about 10-100°C at 5-10 minutes time-intervals.

3.2 Orthoenstatite

before heating

Any remarkable microtextures, such as twinnings, stacking faults, or APB's, were not observed in both the synthetic and the natural specimens before heating under the HTTEM.

natural orthoenstatite

Figure 4 shows the temperature-time diagram of the heating experiment of the natural orthoenstatite. During the heating experiment, no significant change was observed until 1080°C (Figures 5a and 5b). When the temperature was raised to 1140°C, the lineations like twinnings or stacking faults suddenly appeared parallel to the *c* axis (Figure 5c) The lineation texture extended all over the specimen with the time or a rise in temperature up to 1230°C (Figures 5d, 5e) Some extra reflection spots and the diffuse streaks parallel to the a^* direction were observed in the diffraction pattern in addition to the reflection spots of *ortho* (*e.g* , Figure 5e) The extra spots are indexed as *clino(C)*, not *proto*. However, this *clino(C)* was not be identified in the electron micrographs because of the quite minor phase in a fine-scale During the heating, the specimen evaporated terribly at such a high temperature

(above 1200°C) Forsterite patches were sometimes formed by incongruent vaporization of enstatite (Figure 6) This incongruent vaporization is consistent with the vaporization experiments of enstatite at low pressures by Mysen and Kushiro (1988)

After cooling to the room temperature (Figure 5f), most parts of the specimen has been evaporated and lost. The rest of the specimen, survived from the vaporization, remained to be almost as it was before the heating, except for the generation of the (100) stacking faults. These stacking faults contribute to the diffuse streaks in the diffraction pattern parallel to the a^* direction. In some regions of the specimen, the orthoenstatite coexisted with low-clinoenstatite probably transformed from high-clinoenstatite and euhedral crystals of forsterite (Figure 7) Judging from the changes in the diffraction pattern, the *ortho*-to-*clino(C)*-to-*clino(P)* phase transformation occurred although unconfirmed by its direct observation for imaging.

synthetic orthoenstatite

In case of the synthetic specimen, a similar process as in the natural orthoenstatite was observed during the heating, *i.e.*, the phase transformation to *clino(C)* started at almost the same temperature (1140°C) Figure 8 shows the temperature-time diagram of the experiment. The

vaporization of the specimen was more seriously at high temperatures than the case of the natural specimen. As the result, it was impossible to observe the texture and the transformation process in the damaged specimen during and after cooling.

In both the synthetic and the natural specimens, the phase transformation to *proto* was not observed even above 1200°C for more than one hour.

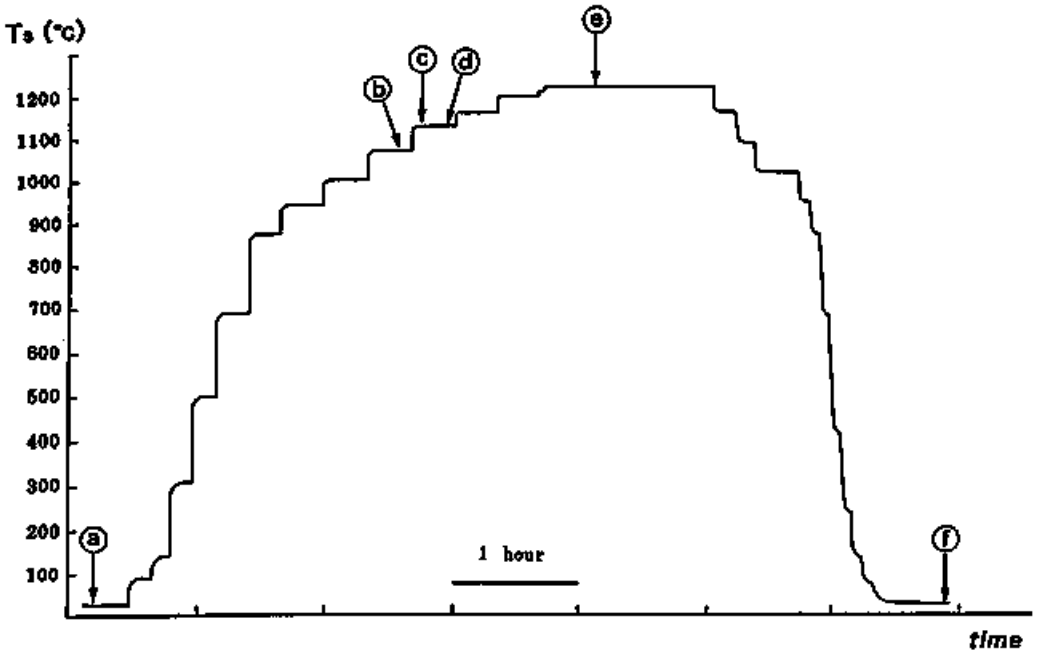

Figure 4. Temperature-time diagram of the heating experiment of the natural orthoenstatite. The signs (a) to (f) correspond to the points where each electron micrograph of Figure 5 was taken.

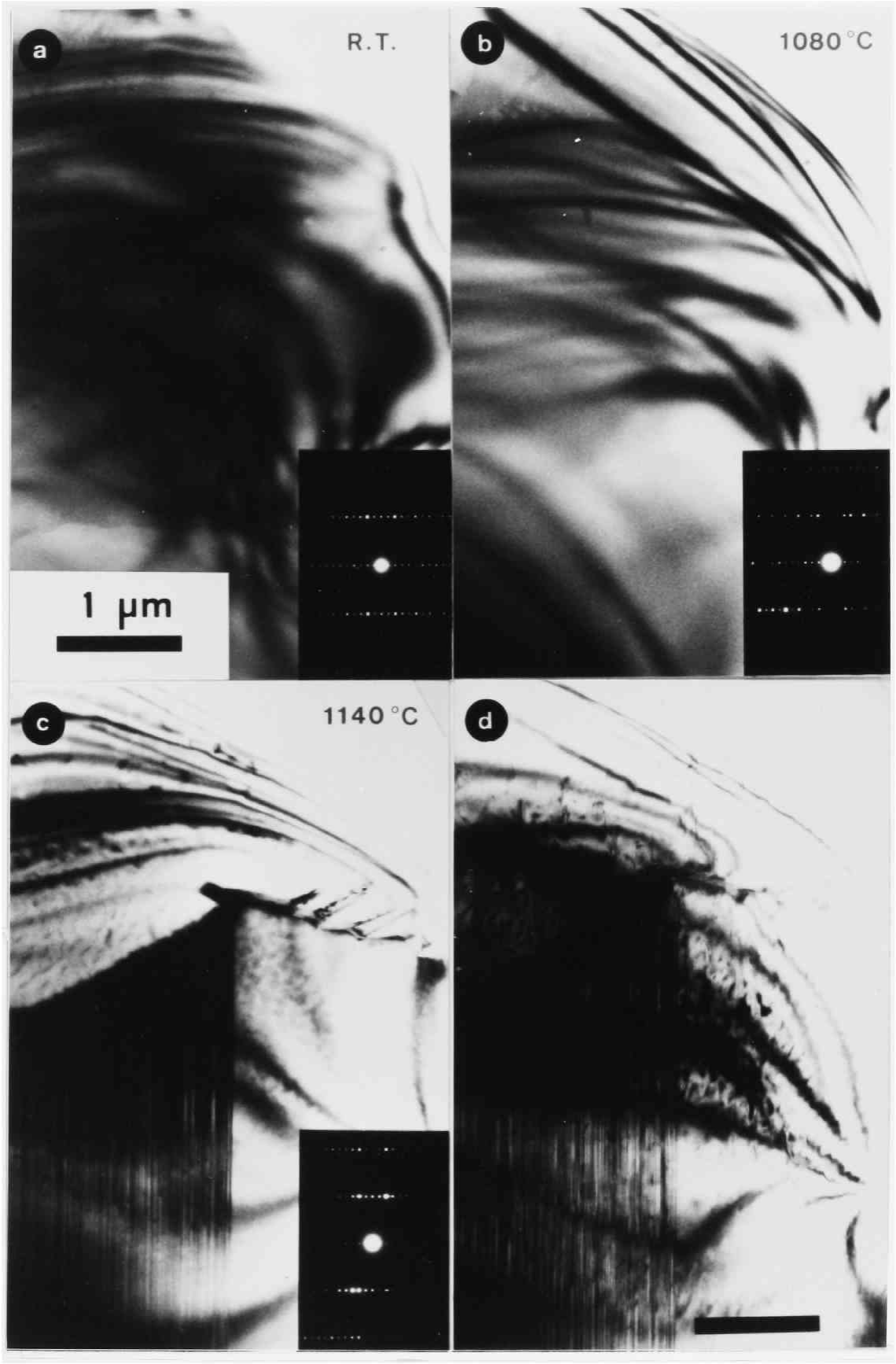
a
R.T.
1 μm
b
1080 °C
c
1140 °C
d

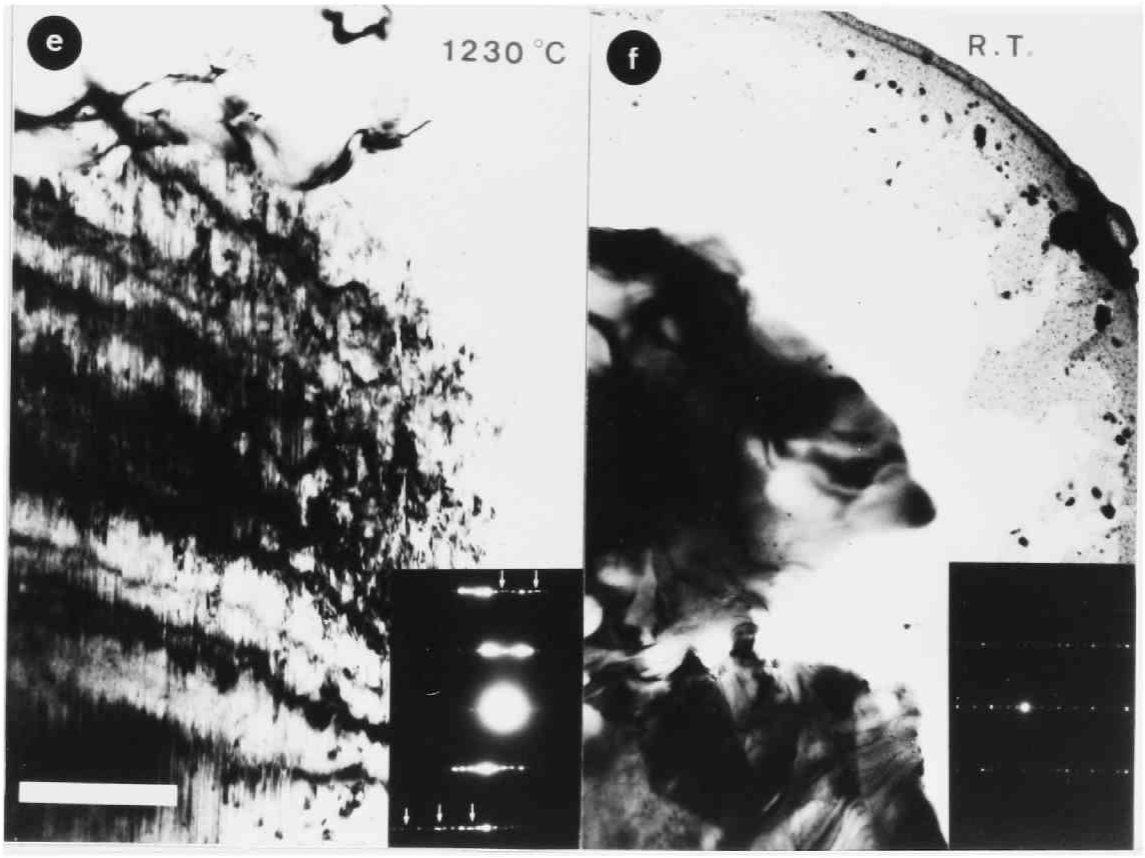

Figure 5. A sequence of bright-field electron micrographs of the heating experiment of the natural orthoenstatite. (a) at the room temperature; (b) upon heating at 1080°C no significant change occurs; (c) upon heating at 1140°C the (100) stacking faults suddenly appear; (d) with the lapse of time at the same temperature the stacking faults gradually extend; (e) upon heating at 1230°C the stacking faults rapidly extend over the most parts of the specimen, the additional reflection spots of high-clinoenstatite (indicated by white arrows) are observed in the right-down diffraction pattern ; (f) after the cooling to the room temperature the most parts of specimen has been evaporated and lost.

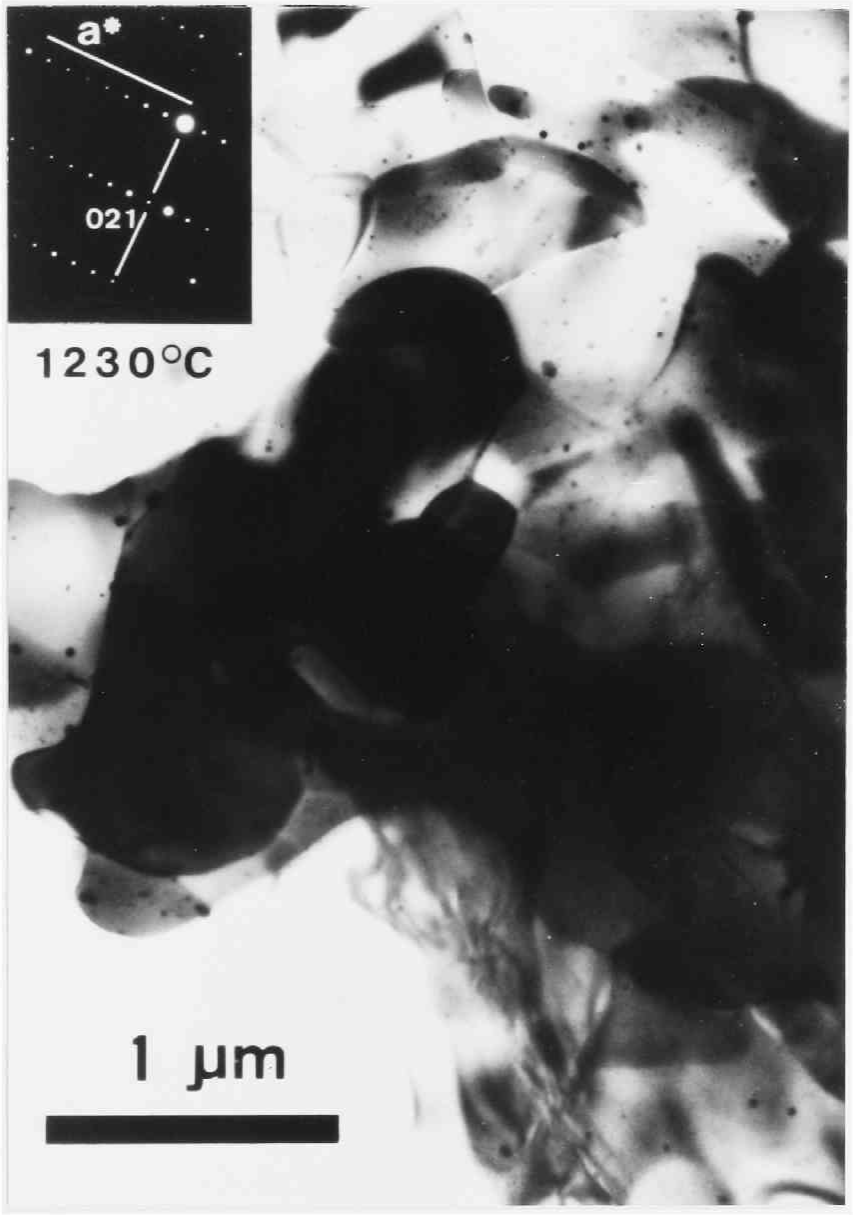

Figure 6. Electron micrograph of forsterite patches formed by incongruent vaporization of the orthoenstatite specimen at above 1200°C. An electron diffraction pattern was taken from one of those grains.

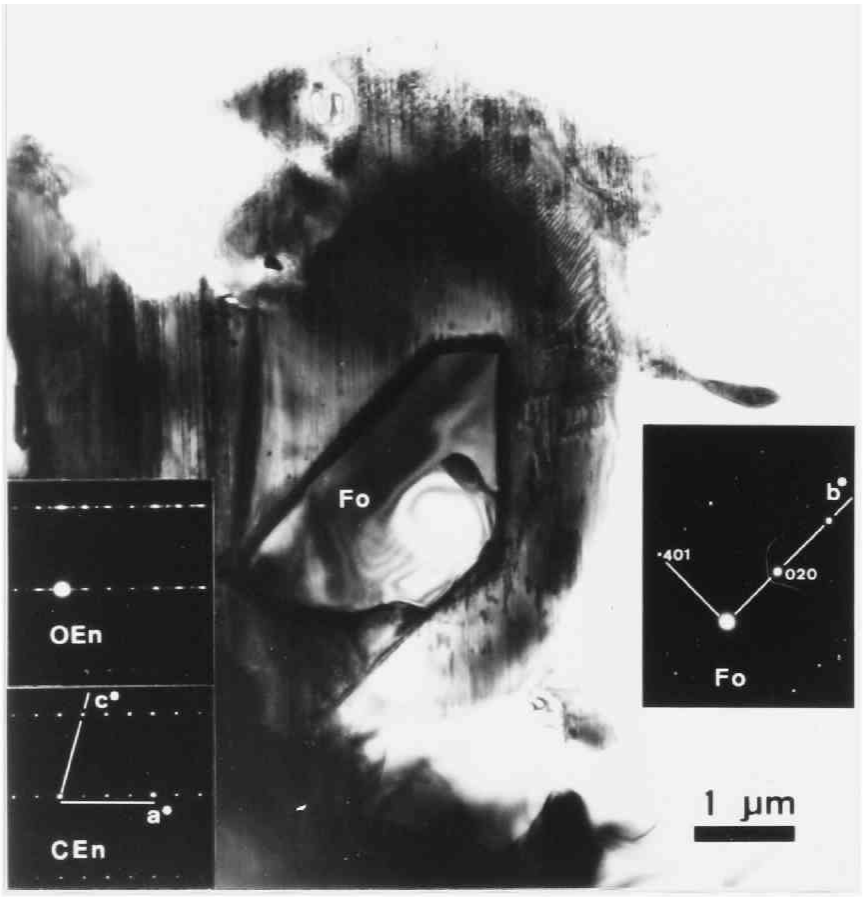

Figure 7 Electron micrograph and electron diffraction patterns showing the coexistence of orthoenstatite, clinoenstatite and forsterite after cooling to the room temperature. The euhedral crystal of forsterite were formed by incongruent vaporization of the starting enstatite specimen at high temperatures under a high vacuum condition during the HTTEM study.

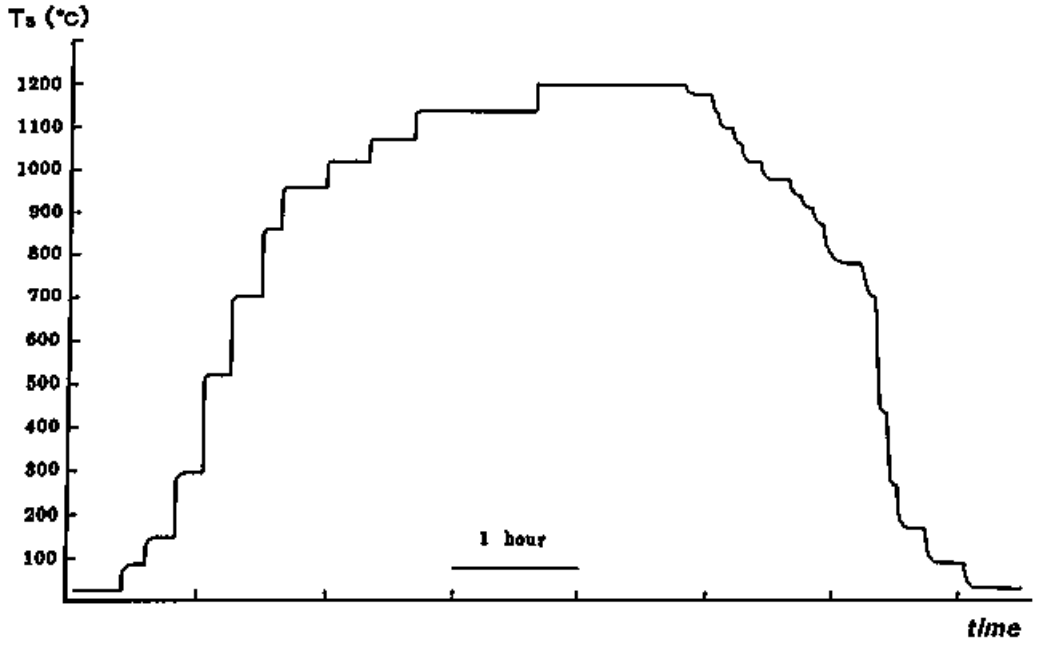

Figure 8. Temperature-time diagram of the heating experiment of the synthetic orthoenstatite.

3.3 Clinoenstatite

before heating

Both the starting specimens of the synthetic and the natural clinoenstatites have fine (100) polysynthetic twins (Figures 10a and 19a) formed by quenching from protoenstatite No APB was observed in both samples before heating under the HTTEM.

natural clinoenstatite

Figure 9 shows the temperature-time diagram of the first heat treatment of the natural clinoenstatite. During the heating, no significant change was shown until about 1110°C when lamellae of *clino(C)*, oblique to the (100) twin planes, suddenly appeared. The lamellae are symmetrical through (100) twin plane, resulting in the herringbone-like texture (Figure 10b) However, any changes in the (100) polysynthetic twins were not observed. The herringbone-like texture is obviously the coexistent texture of *clino(P)* and *clino(C)* with the sharp interfaces between them (Figure 11) The boundaries between *clino(P)* and *clino(C)* (hereafter *P/C* interfaces) are determined to be approximately parallel to $(30\bar{1})$ by measuring the orientation relative to the corresponding diffraction pattern and applying stereographic technique. The *P/C* interface seems to be quite coherent because no dislocations were observed.

At the coexistent stage, as the lamellae of *clino(C)* became thicker, those of *clino(P)* became thinner within a few tens of seconds after temperature changes, and became stagnant at the constant temperatures. Upon further heating, *clino(P)* transformed completely to *clino(C)* at about 1230°C and the herringbone-like texture disappeared (Figure 10c)

When the sample was cooled after the heating at 1230°C for about 30 minutes, the *clino(C)*-to-*clino(P)* phase transformation started and the herringbone-like texture started to appear again at about 1110°C, and the texture disappeared at about 950°C (Table 1)

Any changes in the (100) polysynthetic twins were not detected throughout the HTTEM observation. Any additional defects (*e.g.* slip, dislocation, transformation twin) were not observed except for APB's.

After the first heating experiment, the APB's were observed at the room temperature (Figure 12) Most of them are approximately parallel to $(30\bar{1})$ When the same specimen was heated again in the subsequent heat treatment, the lamellae of *clino(C)* started to grow from the APB's (Figure 13)

Repetition of the heating experiments of the natural specimen has been done several times (Figures 14-16) and the reproducibility of the phase transformation has been confirmed. However, there is an apparent change in the hysteresis loops of the phase transformation. The percent-transformation curves, in a diagram of the volume ratio

transformed vs. temperature, are shown in Figures 17a and 17b on the first and fourth heat treatments, respectively. Each set of two curves on both the heating and the cooling shows the transformation hysteresis loop. The hysteresis loop seems to become smaller as the repetition of the heating experiments.

synthetic clinoenstatite

The temperature-time diagram of the heating experiment is shown in Figure 18 In the synthetic specimen, the same herringbone-like texture as that in the natural specimen appeared at 1200°C on heating (Figure 19b), about 100°C higher than the temperature for the natural one, and disappeared at 1240°C (Figure 19c) Any changes in the (100) polysynthetic twins were not detected. On cooling, the herringbone-like texture began to appear at 1120°C and disappeared at about 950°C (Table 1) Any additional defects (*e.g.* slip, dislocation, transformation twin) were not observed.

The subsequent reheating experiments using the same specimen could not be carried out because the recovered specimen from the first heat treatment had the dreadful damage of the specimen by heating and/or by electron exposure.

Protoenstatite, a stable phase at high temperatures, was not observed in both the synthetic and the natural specimens by heating even more than 1200°C for 1 hour.

The characteristic temperatures (see Figure App.-1) of the phase transformations in both the synthetic and the natural clinoenstatite are summarized in Table 1

Table 1. Temperatures of the *P–C* transformations

Characteristic temperatures, thermal hystereses and *To* temperatures (see Appendix) of the clinopyroxenes using in this HTTEM study are summarized below. For example, *As* of synthetic clinoenstatite is laid between 1140°C and 1200°C.

Specimen	characteristic temperatures				Δ*1 (°C)	*To*2 (°C)
	As (°C)	*Af* (°C)	*Ms* (°C)	*Mf* (°C)		
clinoenstatite (synthetic)	1200 ⋮ 1140	1240 ⋮ 1200	1160 ⋮ 1120	(890) ⋮ 840	+80 ⋮ -20	1180
clinoenstatite (natural) 1st heating	1110 ⋮ 1030	1230 ⋮ 1160	1180 ⋮ 1110	1030 ⋮ 950	0 ⋮ -150	1170
2nd heating	1120 ⋮ 1060	1240 ⋮ 1170	1190 ⋮ 1120	?	0 ⋮ -130	
3rd heating	1110 ⋮ 1040	---- ----	---- ----	1040 ⋮ 970	--- ---	
4th heating	1060 ⋮ 1030	1200 ⋮ 1190	1150 ⋮ 1120	1040 ⋮ 970	-60 ⋮ -120	
pigeonite 1st heating	960 ⋮ 870	1030 ⋮ 1000	970 ⋮ 940	880 ⋮ 840	+20 ⋮ -100	1000
2nd heating	890 ⋮ 840	1030 ⋮ 1000	1060 ⋮ 1000	880 ⋮ 830	-110 ⋮ -220	

*1: $\Delta = A_s - M_s$

*2: $T_o = (A_f + M_s)/2$

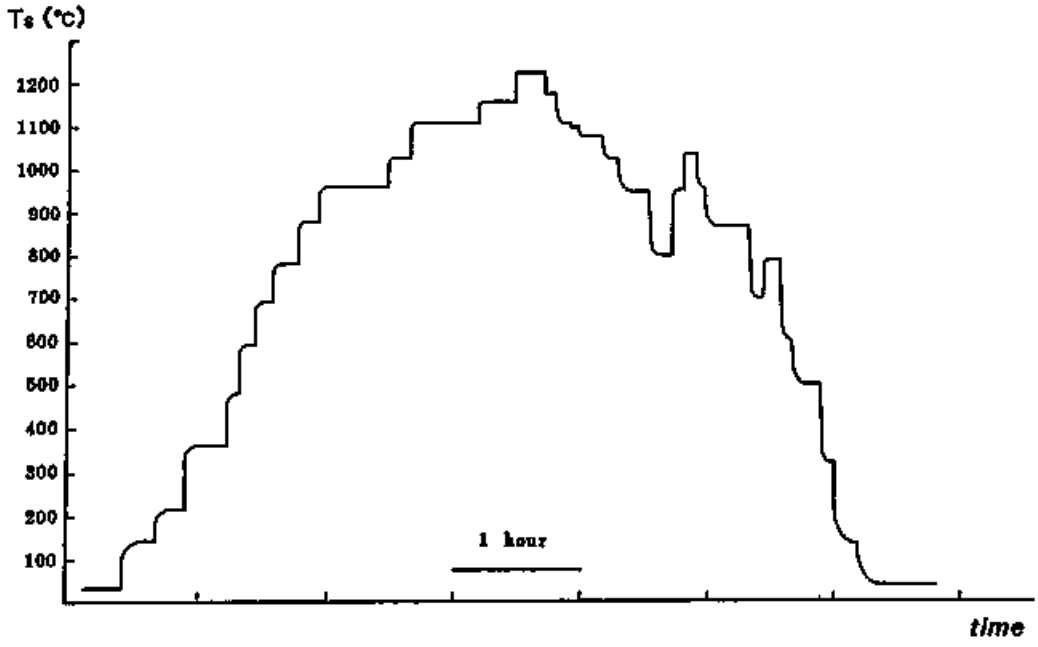

Figure 9. Temperature-time diagram of the first heat treatment of the natural clinoenstatite.

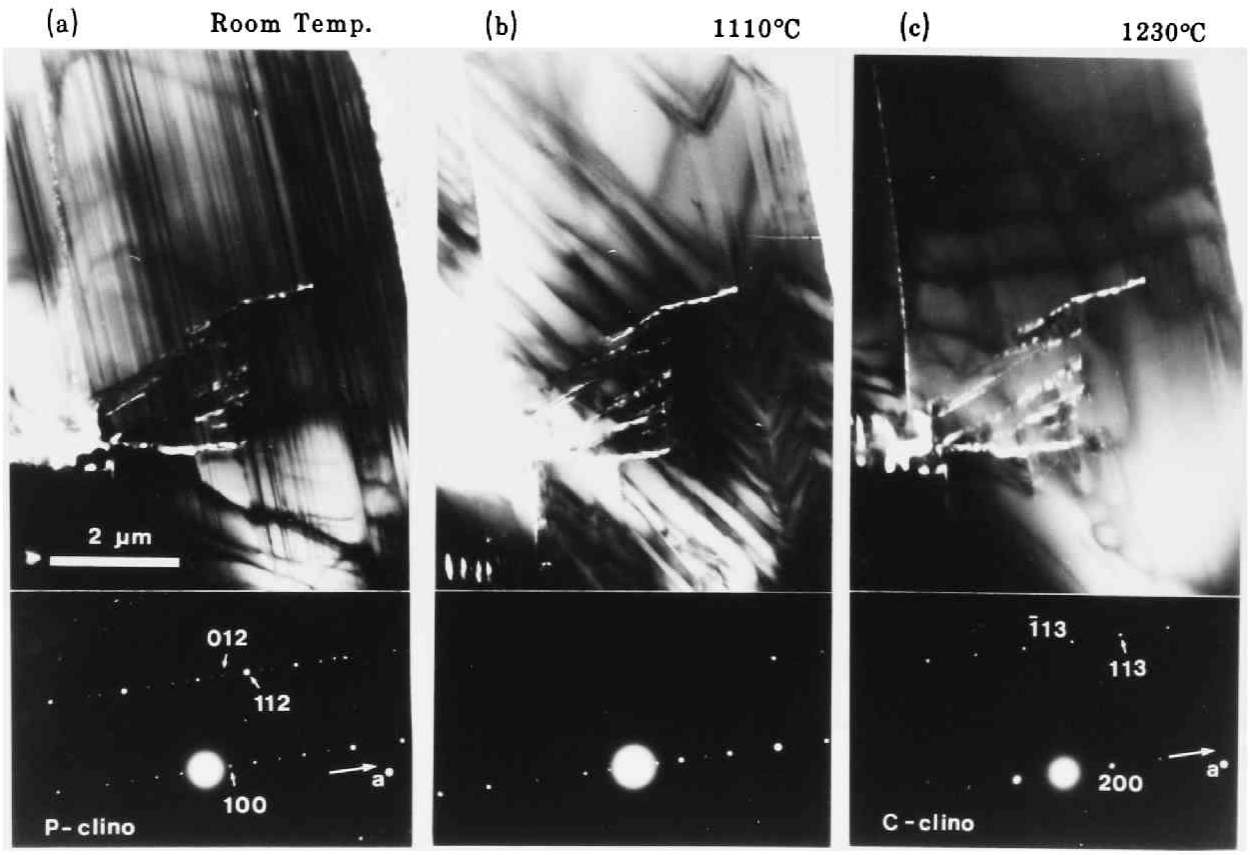

Figure 10. A set of bright-field electron micrographs and electron diffraction patterns of the $P2_1/c$-to-$C2/c$ phase transformation of the natural clinoenstatite on the heating under the HTTEM. (a) at the room temperature; (b) upon heating at 1110°C the phase transformation starts and the resulting 'herringbone'-like pattern appears; (c) upon heating at 1230°C the transformation completes and the 'herringbone'-like pattern disappears.

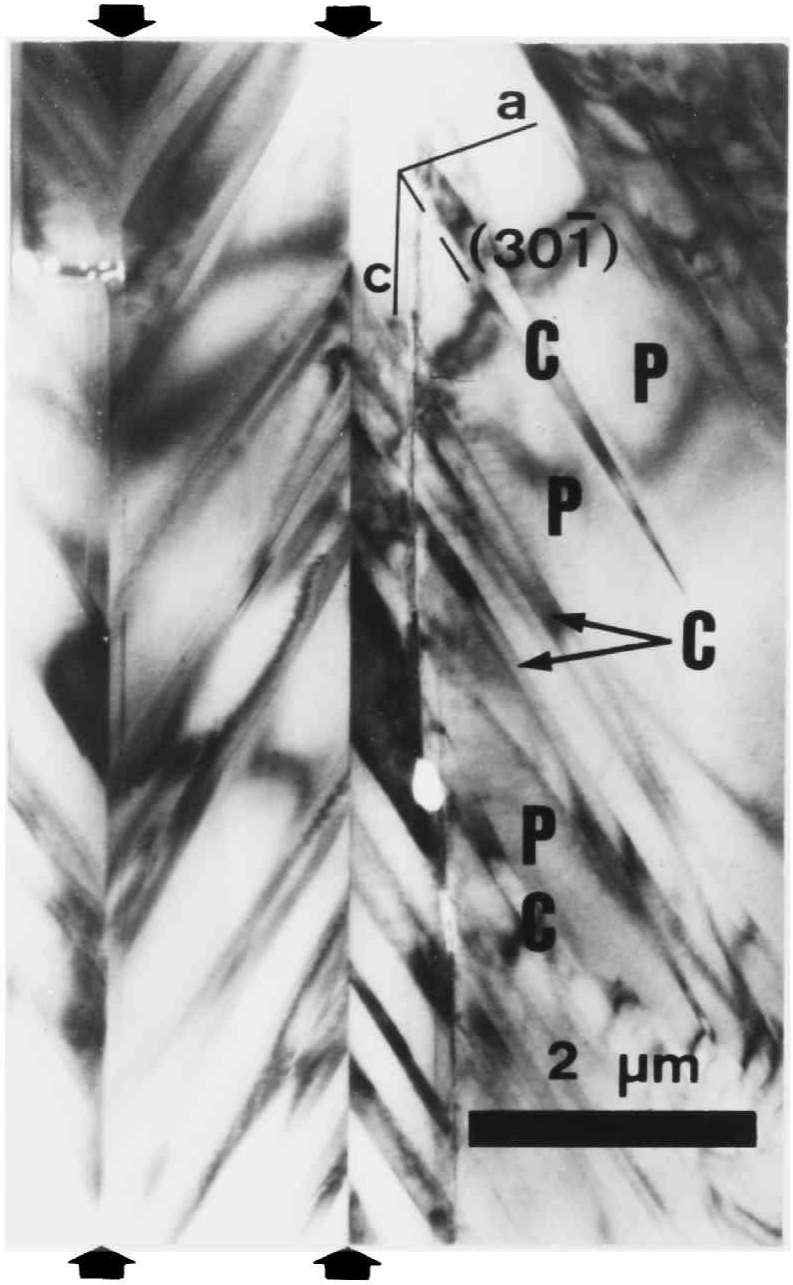

Figure 11. Electron micrograph of the 'herringbone'-like pattern at 1100°C. The (100) twin boundaries are illustrated by arrows. The 'herringbone'-like pattern is the resulting texture of the coexistence of both low- and high-clinoenstatite (as indicated by 'P' and 'C', respectively) The interfaces between two phases seem to be approximately parallel to (30$\bar{1}$). This was taken in the fourth heat treatment of the natural specimen.

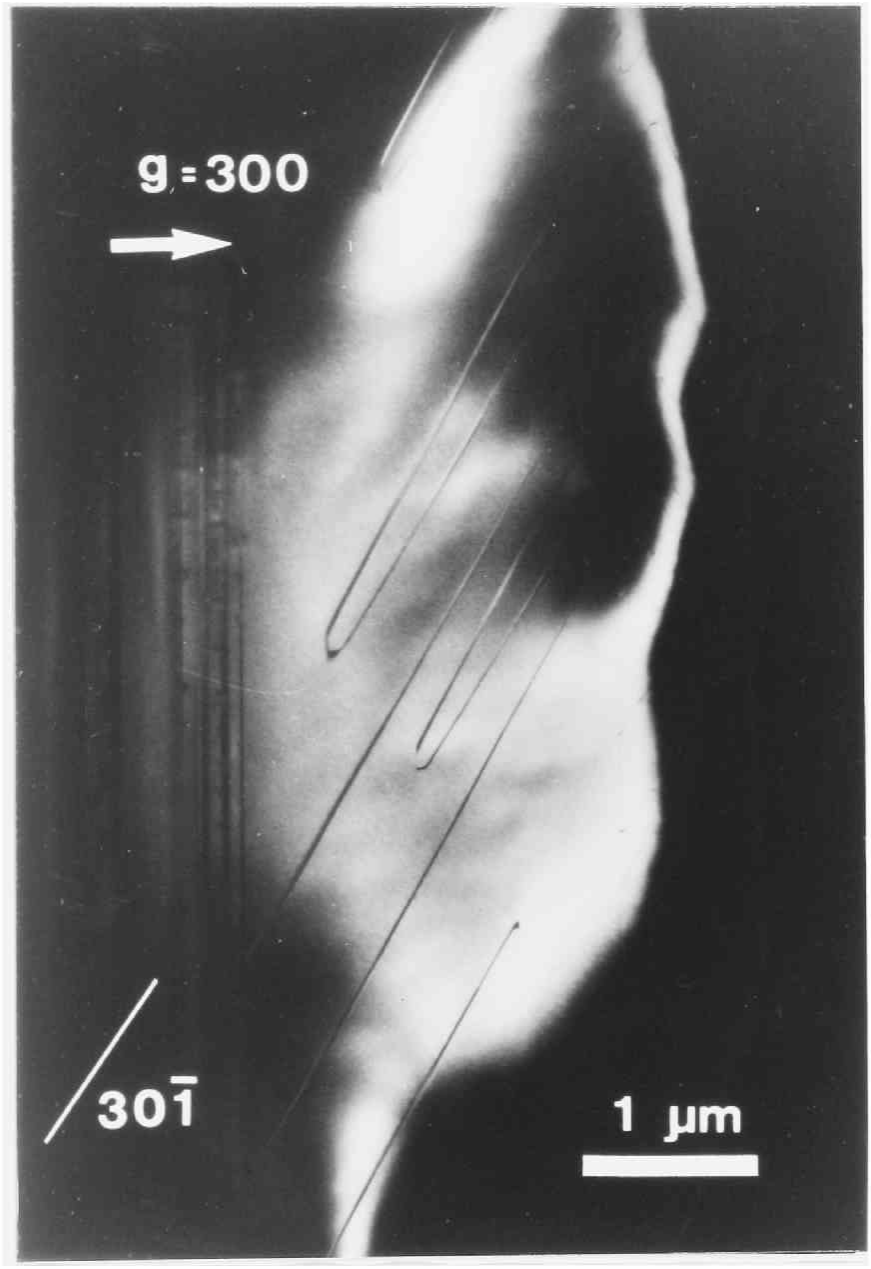

Figure 12. Antiphase boundaries (APB's) in the natural clinoenstatite after the first heat treatment. The most APB's are approximately parallel to (30$\bar{1}$)

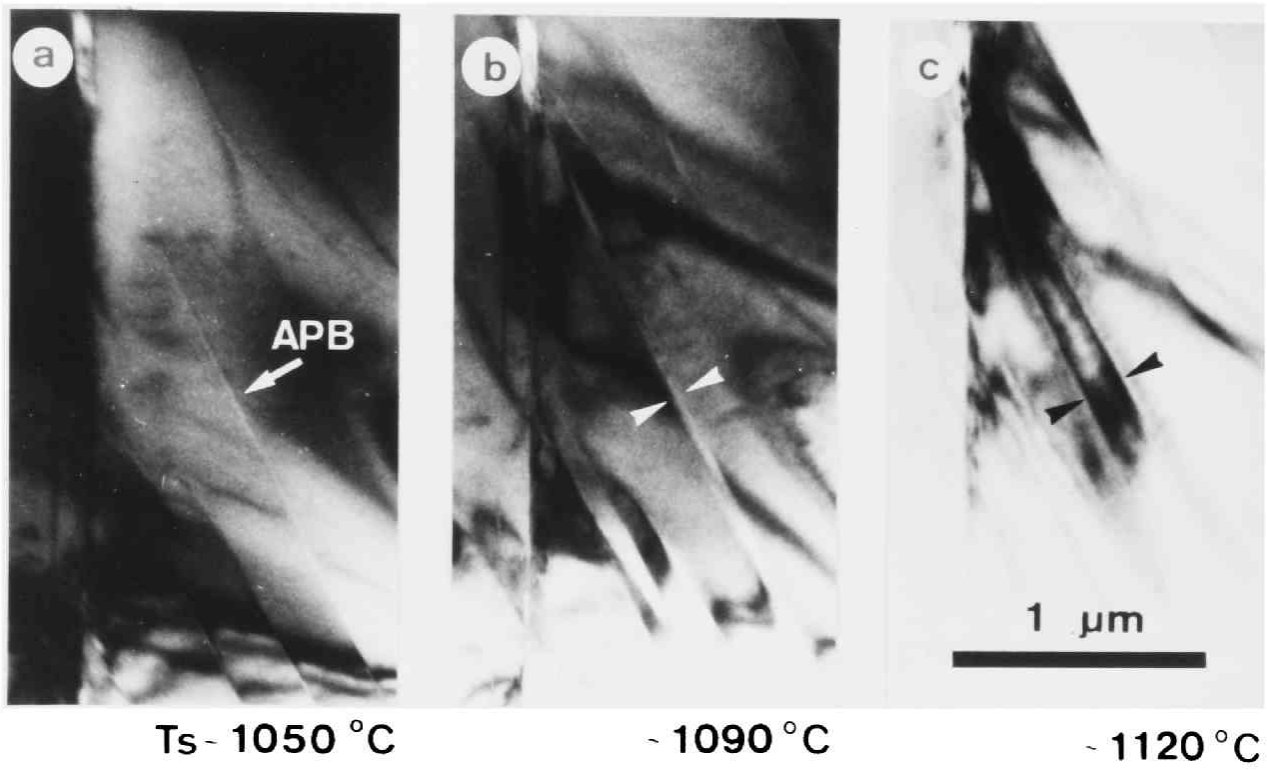

Figure 13. Nucleation and growth process of high-clinoenstatite ($C2/c$) from the parent phase of low-clinoenstatite during the low-to-high clinoenstatite phase transformation. This process makes use of the APB's formed during the first heat treatment. The lamella between a set of arrows (b or c) represents high-clinoenstatite growing from the APB, illustrated by an arrow in (a) on the heating. These micrographs were taken in the fourth heat treatment of the natural specimen.

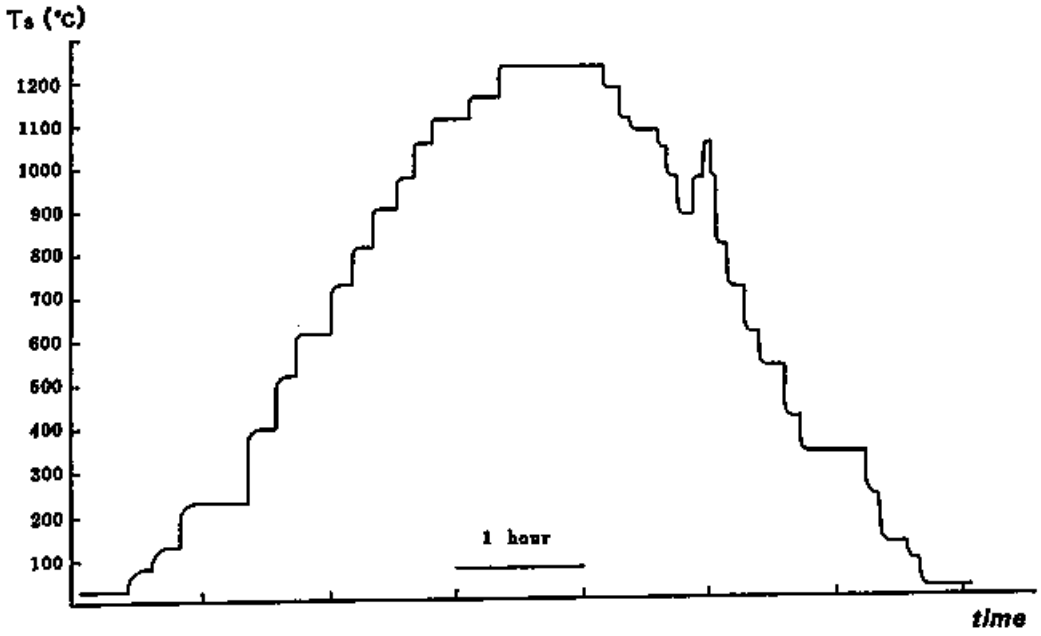

Figure 14. Temperature-time diagram of the second heat treatment of the natural clinoenstatite.

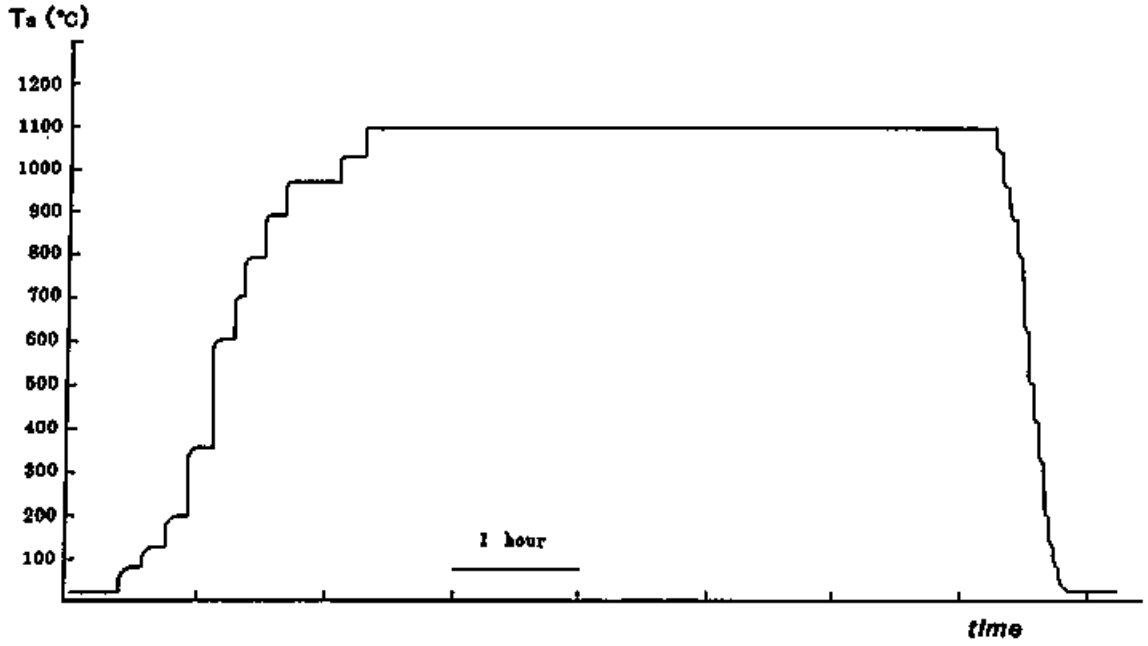

Figure 15. Temperature-time diagram of the third heat treatment of the natural clinoenstatite.

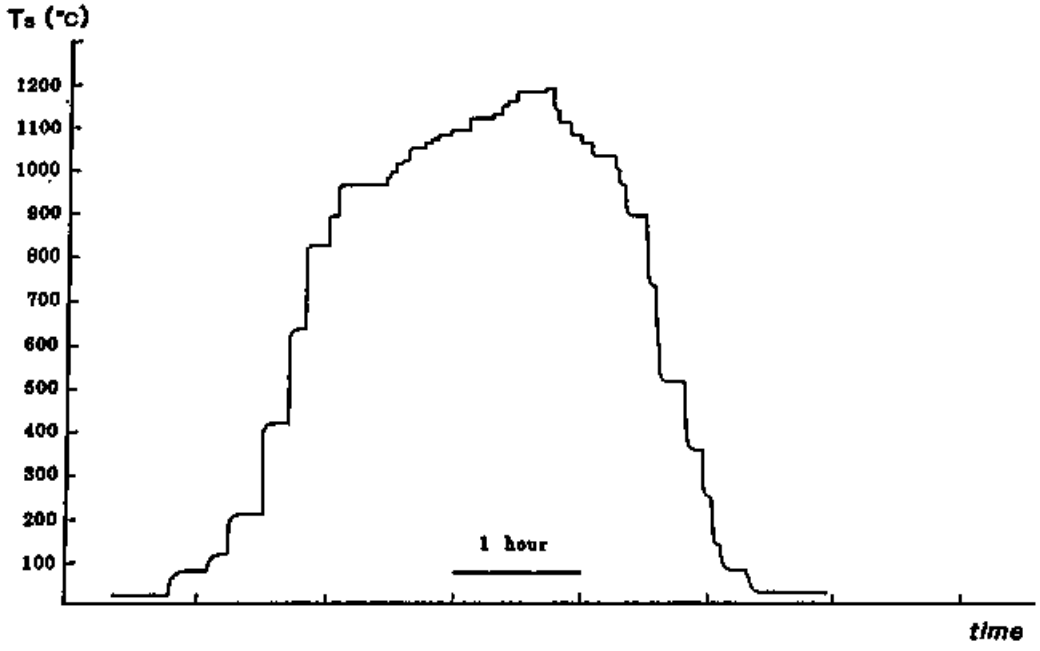

Figure 16. Temperature-time diagram of the fourth heat treatment of the natural clinoenstatite.

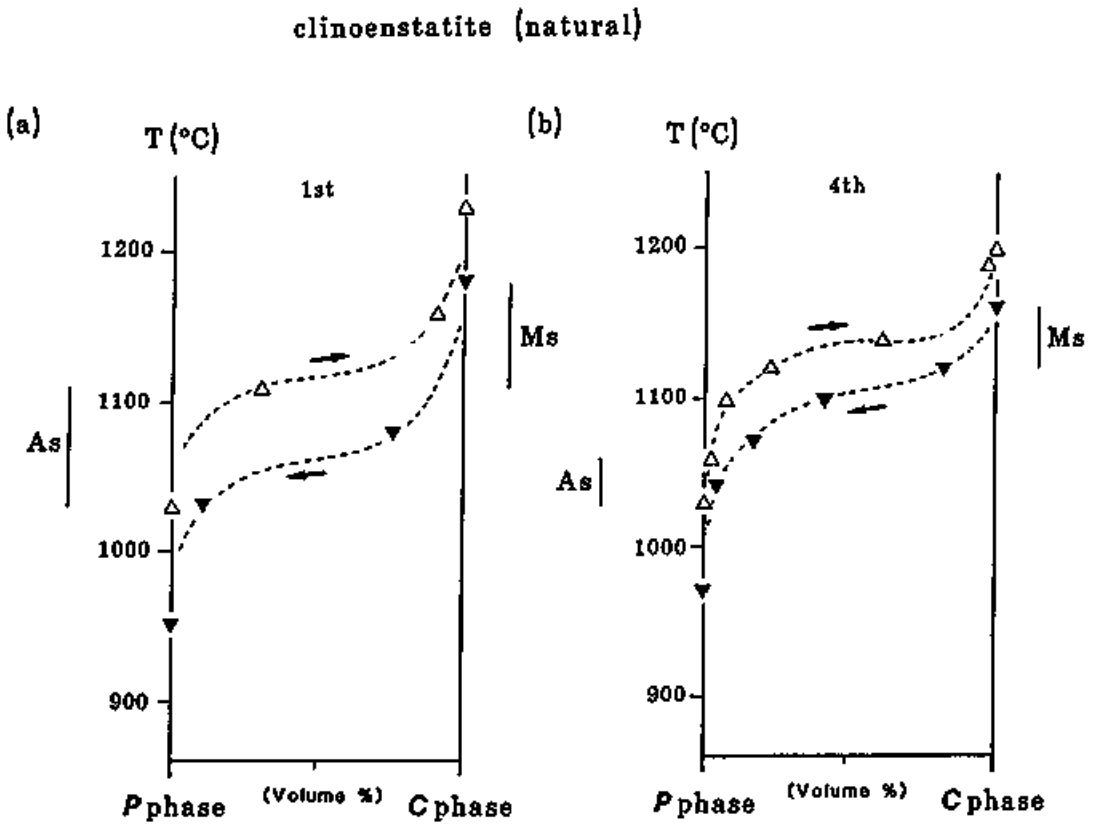

Figure 17. Percent-transformation curves in (a) the first and (b) the fourth heat treatment of the natural clinoenstatite. The percentages are shown by the volume ratio transformed. The hysteresis loop in the fourth treatment becomes narrower than that in the first treatment. The temperature ranges, in which A_s and M_s (transformation start temperatures; see Appendix) are laid, are also shown.

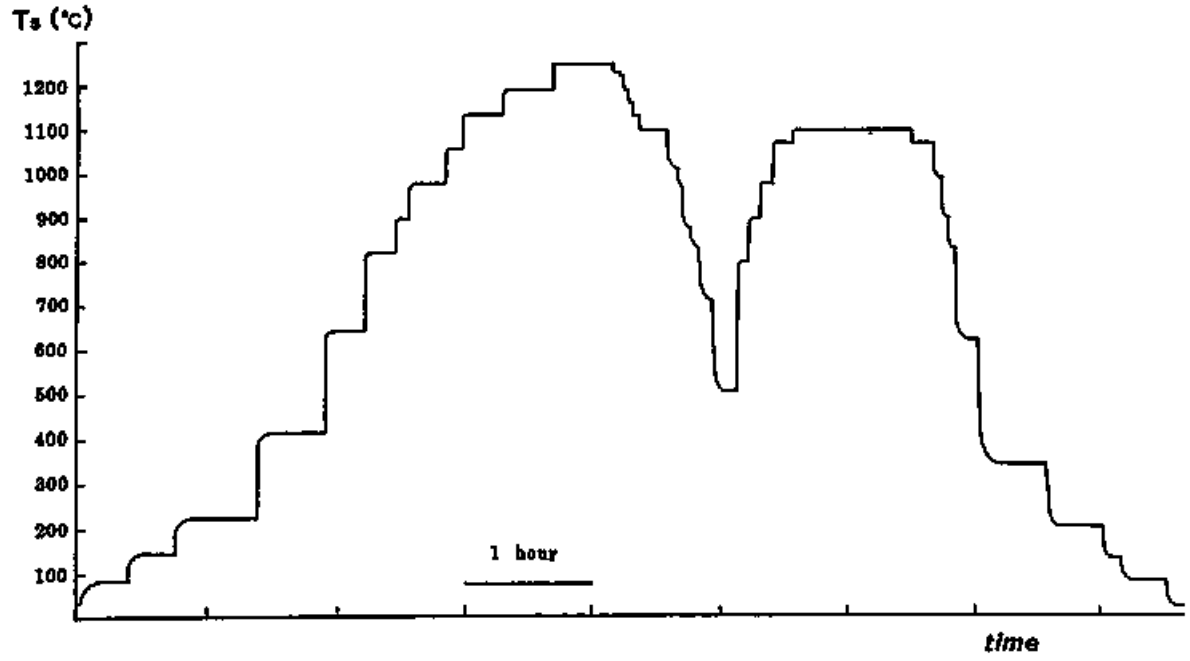

Figure 18. Temperature-time diagram of the heating experiment of the synthetic clinoenstatite.

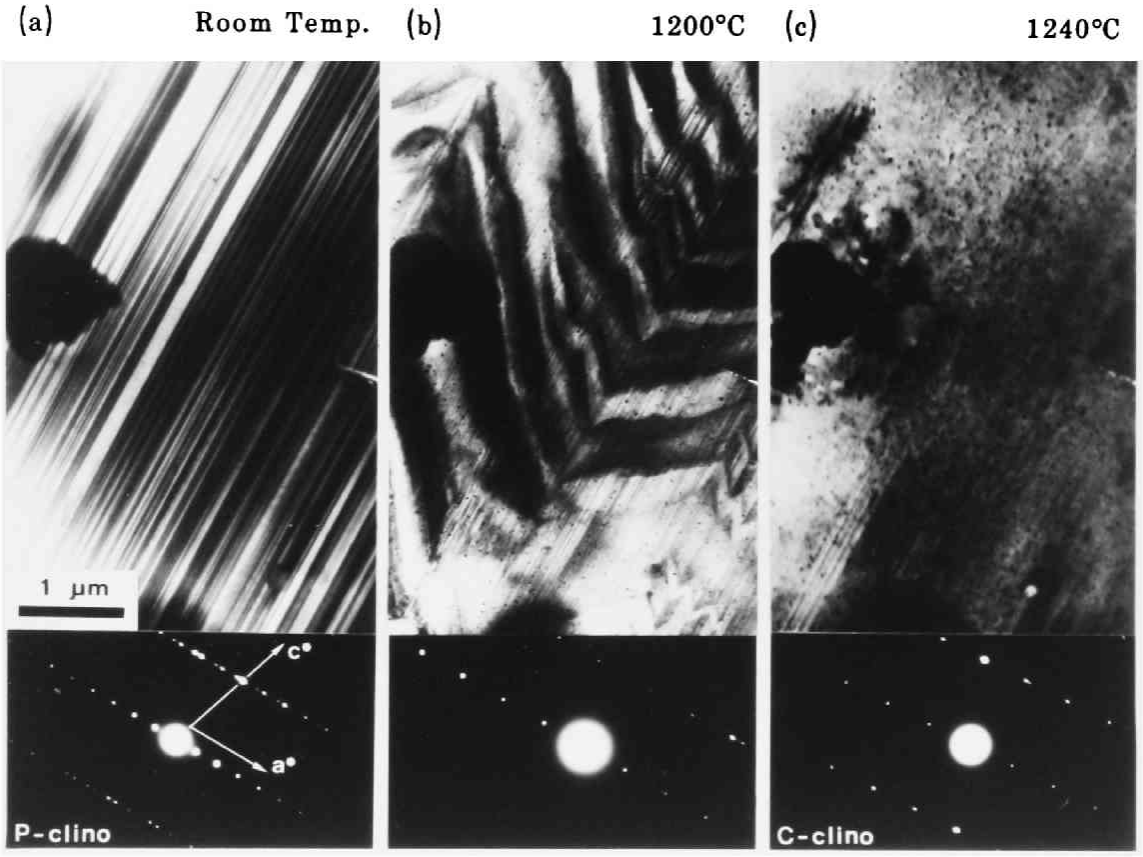

Figure 19. A set of bright-field electron micrographs and electron diffraction patterns of the $P2_1/c$-to-$C2/c$ phase transformation of the synthetic clinoenstatite on the heating under the HTTEM. (a) at the room temperature; (b) upon heating at 1200°C the phase transformation starts and the resulting 'herringbone'-like pattern appears; (c) upon heating at 1240°C the transformation completes and the 'herringbone'-like pattern disappears.

3.4 pigeonite

before heating:

The pigeonite specimen contains '001' augite lamellae, about 0.05 - 0.2 μm in thickness (Figure 20) Figure 20 shows a dark-field [g=102] electron micrograph and an electron diffraction pattern of the pigeonite specimen. Because this dark-field electron micrograph was taken using a class (*b*) reflection (*h*+*k*; odd), the visible white contrast is derived only from the $P2_1/c$ structure, and the $C2/c$ structure loses in contrast (black) Therefore, the black stripes in Figure 20 represent the augite lamellae. The APD structure is apparent in the pigeonite host. The APB's elongate to an oblique orientation from the *c* axis and have a sigmoidal shape before heating under the HTTEM. In the central part of the thicker pigeonite lamellae (more than about 0 2 μm thick), fine augite plates are precipitated parallel to '001' at the APB's. In the marginal part of the pigeonite lamellae, named "precipitate free zone" (PFZ) by Carpenter (1978), the straight APB's parallel to the *c* axis are also found. The observed microtextures are quite similar to the slowly-cooled pigeonites in coarse grain dolerites described by Carpenter (1978)

the first heat treatment:

The temperature-time diagram of the first heat treatment of pigeonite is shown in Figure 21 On the heating, no significant change occurred until 960°C when the *clino(P)*-to-*clino(C)* transformation started, *i.e.* *clino(C)* started to grow from APB's as the 'fattening' of the APB's, seemingly nucleated at there (Figure 22a) When the temperature was increased to 1000°C, the *clino(C)* grew thicker (Figures 22b, 22c) The growth of the *clino(C)* ceased within several minutes (longer than the case of clinoenstatite) after temperature changed, and became stagnant with further time (Figure 23) Upon heating further to 1030°C, the *clino(P)* became smaller rapidly (Figure 22d) and finally vanished. On the cooling, the *clino(C)*-to-*clino(P)* transformation started at 940°C, proceeded as the temperature decreased, and completed in the range of 880°C to 840°C (Figures 24a-d) Figure 25 shows a summary of the changes of the pigeonite in the first heat treatment.

At the coexistence stage of *clino(P)* and *clino(C)* of pigeonite (Figure 25b), the *P/C* interfaces had a sigmoidal shape, not straight as the case of clinoenstatite. The *P/C* interfaces are oblique from the *c* axis and some of them can be approximately indexed as $(10\bar{1})$, $(20\bar{1})$ or $(30\bar{1})$, as shown in Figure 22c. A region of *clino(P)* surrounded by both two coarse augite lamellae and two *P/C* interfaces is designated as "*P*-cluster" During the heating process, the *P*-clusters

were usually composed of a single domain of *clino(P)*. During the cooling, on the contrary, almost all of the *P*-clusters were composed of several domains of *clino(P)* These domains were bounded each other by newly formed APB's whose orientations were approximately parallel to the *c* axis as shown in Figures 24b and 24c The APB's oblique to the *c* axis, which were commonly observed before the heating, formed at the final stage of the *clino(C)*-to-*clino(P)* phase transformation, seemingly as the traces of the *P/C* interfaces.

After the cooling to the room temperature, most of the APB's were seemingly changed to be straight and approximately parallel to the *c* axis (Figure 25 or Figure 26), as pointed out by Fujino *et al.* (1988) The cooling rate of 200-300°C/hour in the present study corresponds to "quench" in the annealing experiments by Fujino *et al.* (1988)

the second heat treatment:

The same specimen was heated again (Figure 27) and the same process of the *P–C* phase transformation as the first heat treatment was observed. The coexistent texture of *clino(P)* and *clino(C)* in the second heat treatment is shown in Figure 28. As seen in Figure 28b, the APB's parallel to the *c* axis, which was newly formed in the first heat treatment, have obviously not any effect on the orientation of the *P/C* interfaces. The orientations of the *P/C* interfaces are unchanged. *Clino(C)* appeared almost at the same position in the first heat treatment. This behaviour in the appearance of high temperature form is similar to that revealed by the *in situ* observation of Van Tendloo *et al* (1989) for anorthite.

There is an apparent change in the hysteresis loops of the phase transformation between the first and second heat treatments. The percent-transformation curves of pigeonite are shown in Figures 29a and 29b, in the first and second heat treatments, respectively In the first heat treatment, a set of the curves on both the heating and cooling shows a large hysteresis loop (Figure 29a) In the second heat treatment, on the other hand, a set of the curves on the heating and on the cooling becomes to superpose upon each other (Figure 29b) As the result, the hysteresis loop in the second heat treatment changed into converge to a single

curve along which the transformation proceeded reversibly on both heating and cooling. This tendency is similar but more remarkable than the case of clinoenstatite.

The characteristic temperatures (see Figure App.-1) of the pigeonite transformations are also listed in Table 1, in company with those of the clinoenstatite

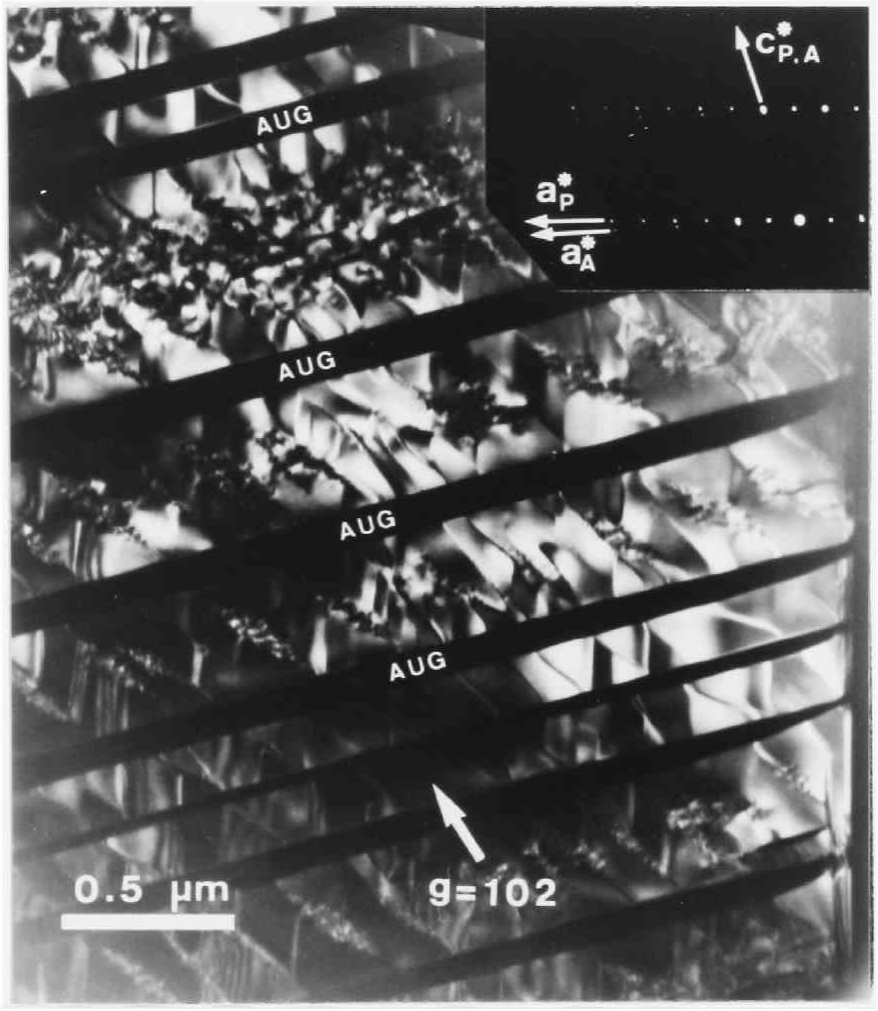

Figure 20. Dark-field [g=102] electron micrograph and electron diffraction pattern of the Hakone pigeonite with coarse, heterogeneously spaced '001' augite lamellae (as shown by 'AUG'). The augite and pigeonite reflections are discrete in the pattern. The arrows in the pattern, show the a^* and c^* axes. Subscripts, 'P' and 'A', represent 'pigeonite' and 'augite', respectively.

Figure 21. Temperature-time diagram of the first heat treatment of the pigeonite.

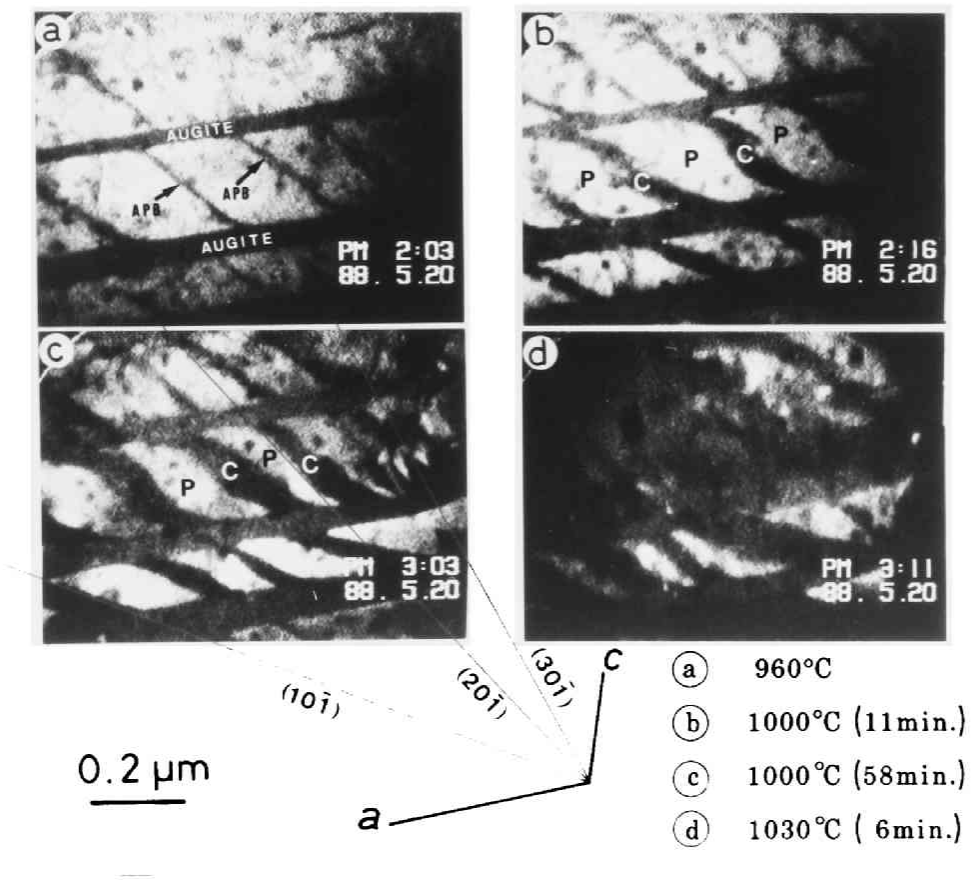

Figure 22. A sequence of dark-field [g=102] electron micrographs (a-d) hard-copied from a video tape of the low-to-high pigeonite phase transformation on the heating in the first heat treatment. The signs, 'P' and 'C', in (b) and (c) represent 'low-pigeonite ($P2_1/c$)' and 'high-pigeonite ($C2/c$), respectively. A region of low-pigeonite (as illustrated by 'P'), surrounded by two coarse augite lamellae and two P/C interfaces, are designated as "P-cluster"

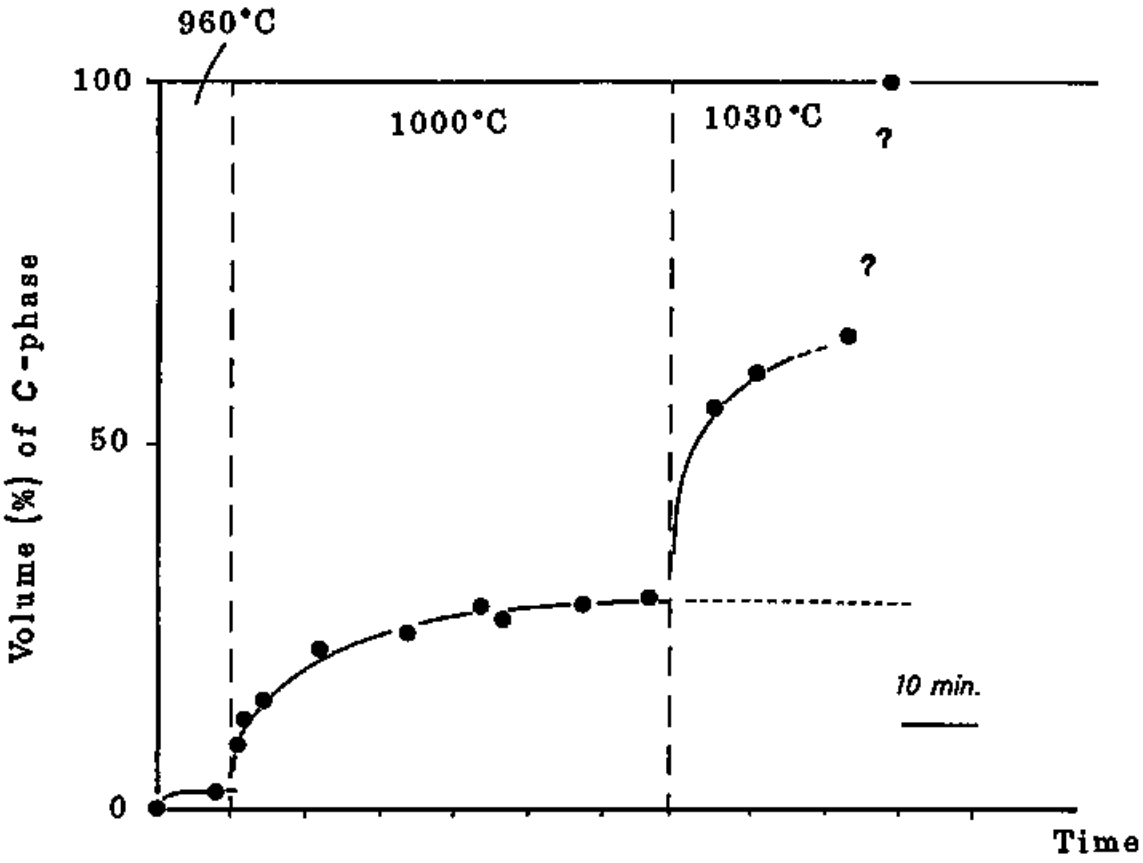

Figure 23. Percentage transformed vs. time diagram on the heating in the first heat treatment of pigeonite. This diagram suggests that the percentage transformed must not increase if the specimen is remained at the constant temperature of 1000°C for much more long times.

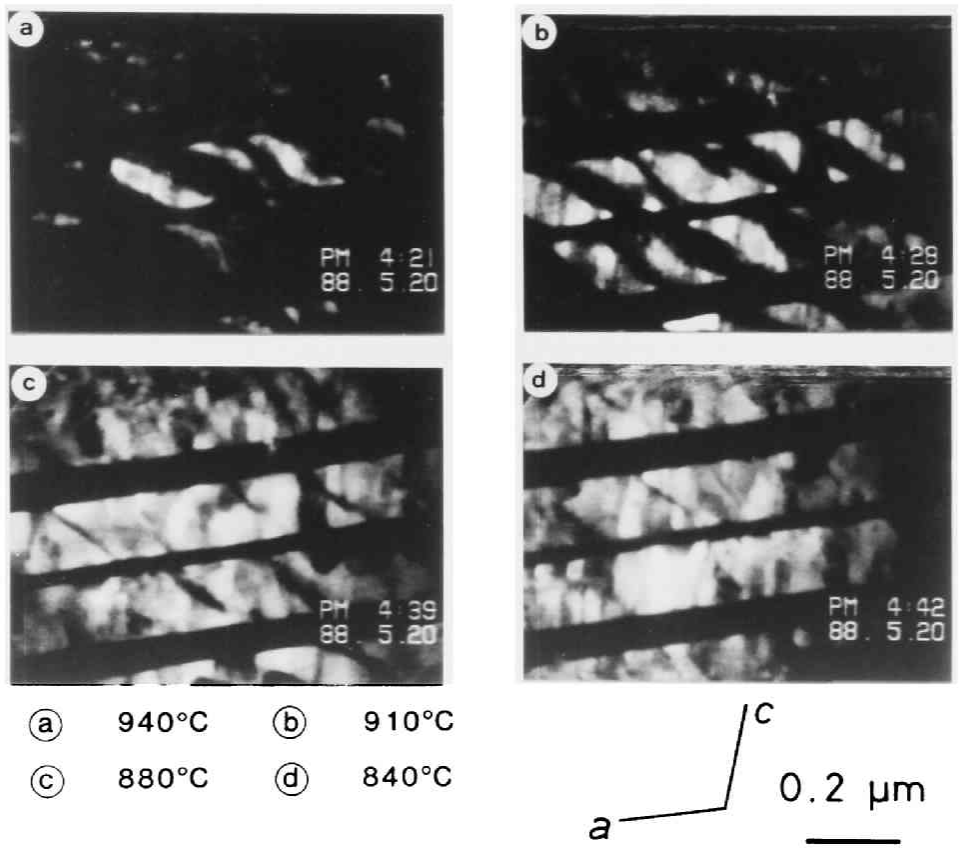

Figure 24. A sequence of dark-field [g=102] electron micrographs (a-d) hard-copied from a video tape of the high-to-low pigeonite phase transformation on the cooling in the first heat treatment.

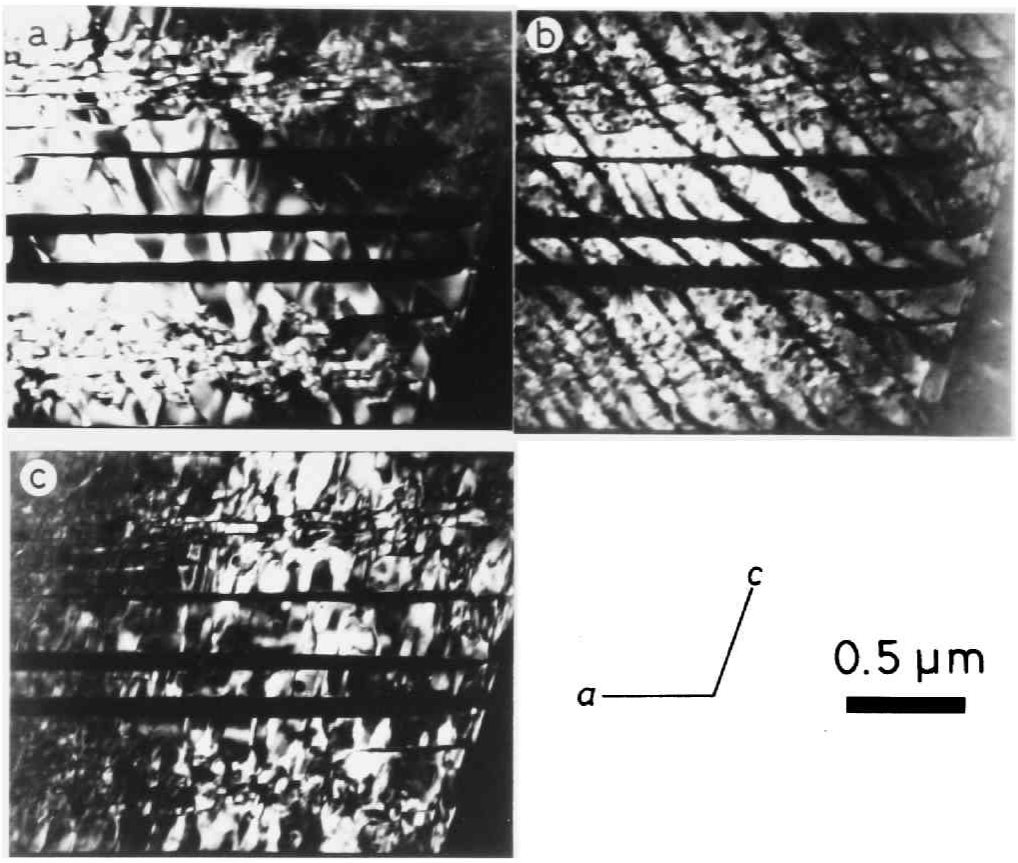

Figure 25. A set of dark-field [g=102] electron micrographs in the first heat treatment of the pigeonite. (a) at the room temperature before heating; (b) *in situ* photographed at 1000°C; (c) at the room temperature after cooling. The coexistence of low and high pigeonites is observed in (b) The change in the orientation of APB's is shown between (a) before and (c) after the heating experiment under HTTEM.

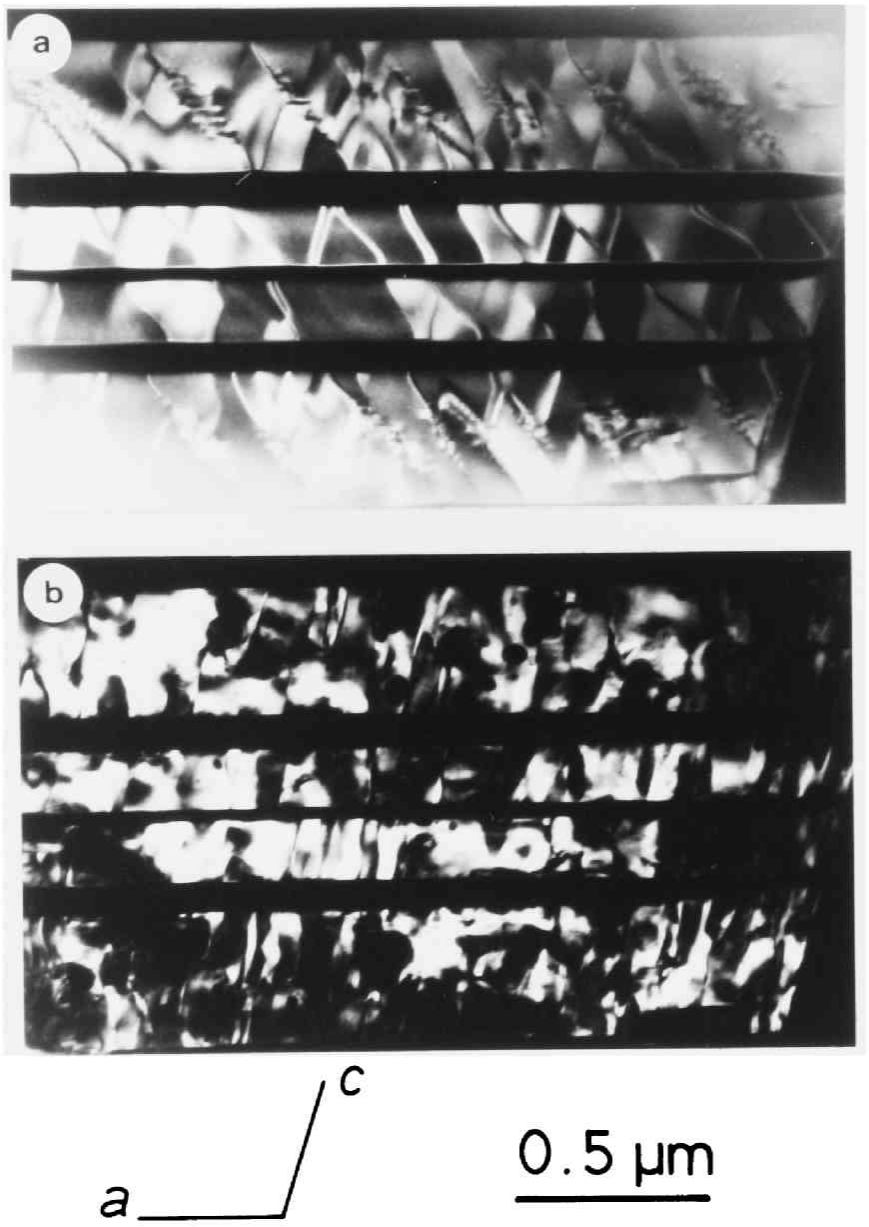

Figure 26. A set of dark-field [g=102] electron micrographs taken at the room temperature showing the change in the orientation of APB's between (a) before and (b) after the first heat treatment of the pigeonite.

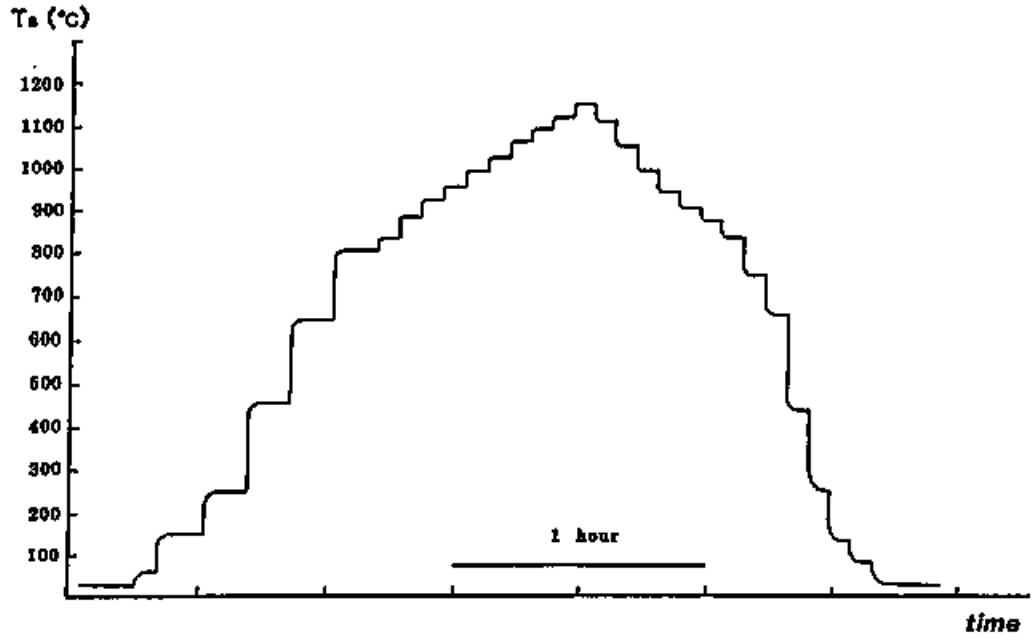

Figure 27. Temperature-time diagram of the second heat treatment of the pigeonite.

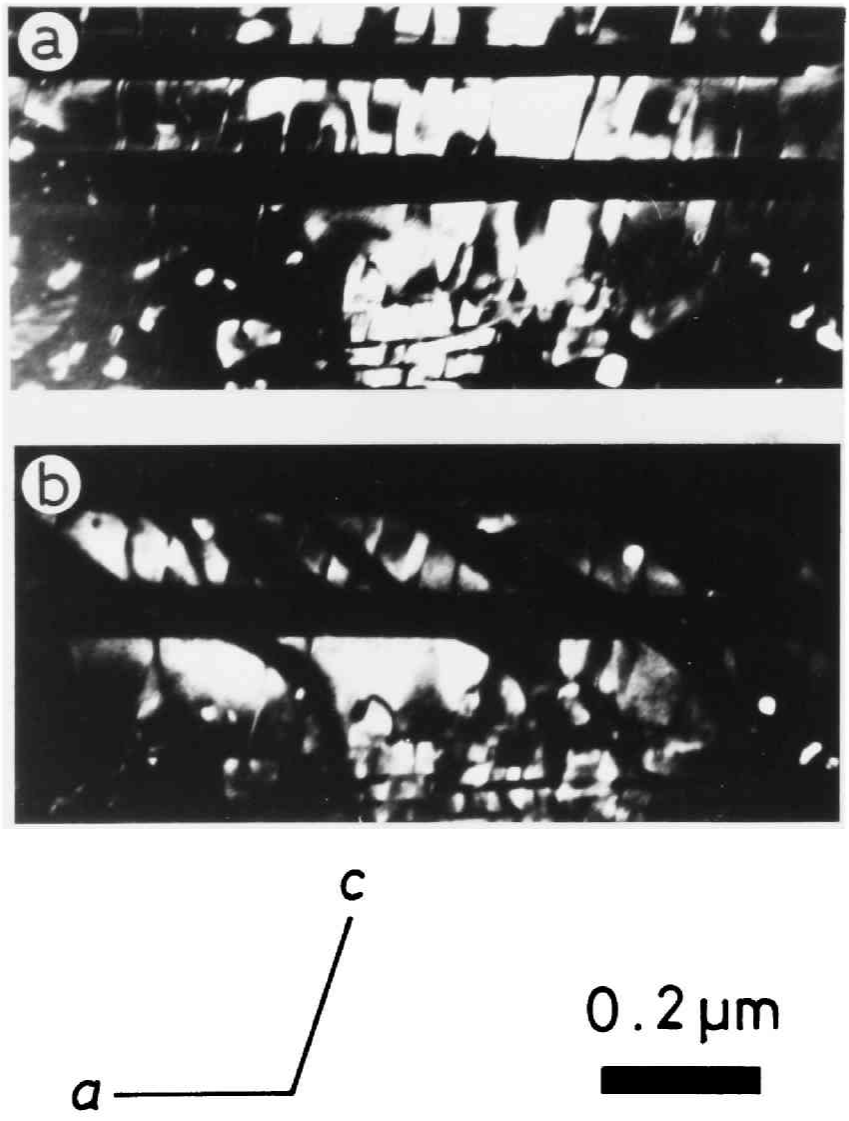

Figure 28. A set of dark-field [g=102] electron micrographs in the second heat treatment of the pigeonite. (a) at the room temperature before the second heating; (b) upon heating at 960°C the orientation of the *P/C* interfaces between low and high pigeonites is unchanged in comparison with the first heat treatment.

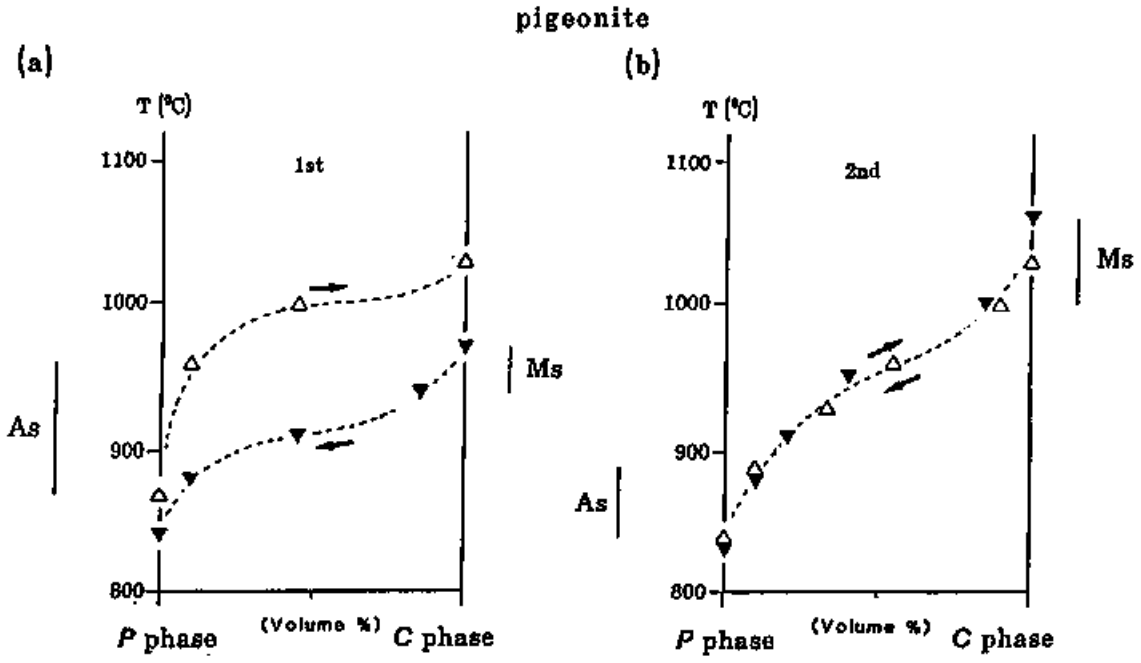

Figure 29. Percent-transformation curves in (a) the first and (b) the second heat treatment of the pigeonite. The percentage are shown by the volume ratio transformed. The hysteresis loop in the second treatment becomes much narrower than that in the first one, and almost converges to a single curve.

4 Discussion

4.1 Polymorphic phase transformation in enstatite

In the present study, both *ortho* and *clino(P)* of enstatite transformed not to *proto* but to *clino(C)*. According to the high temperature X-ray studies by previous investigators (*e.g.*, as summarized in Smith, 1969a; Smyth, 1974a; Murakami *et al.*, 1982), *ortho* always transformed to *proto*. Therefore, the *ortho*-to-*clino(C)* phase transformation for enstatite, as well as for hypersthene and ferrosilite, was observed for the first time in this study Two reasons why the phase transformation to *proto* did not occur are thought; (1) a deficiency of the heating duration and/or (2) an effect of the thermal stress, which are discussed as follow

(1) a deficiency of the heating duration: Smyth (1974a) reported that the *ortho*-to-*proto* phase transformation requires up to several days for completion at a constant temperature of 1200°C, whereas Murakami *et al.* (1982) described that the *ortho*-to-*proto* phase transformation occurred instantaneously at 1100°C. Sadanaga *et al* (1969) showed that the *clino(C)*, which transformed from *clino(P)* after heating up to 1100°C for 10 hours, is an intermediate phase of the *clino(P)*-to-*proto* phase transformation, although Smyth (1974a) described that the *clino(P)*-to-*proto* phase transformation occurs rapidly There is a possibility

of the transformation to *proto* after more heating duration in the present experiments. However, incongruent vaporization to forsterite and melt (silica) occurred quickly at such a high temperature and under a high vacuum condition such as the HTTEM. It was impossible for orthoenstatite to keep the specimen for long time without vaporization at high temperatures under the HTTEM.

(2) an effect of the thermal stress: Protoenstatite is considered to be stable under a stress-free condition at high temperatures (as reviewed in Smith, 1969a) A foil specimen for HTTEM bends by heating probably due to inhomogeneities of the thermal expansion of the specimen. Stress might be generated by this type of the bending. Under such a stress-bearing condition, *clino(C)* may be more stable than *proto*. In fact, *clino(P)* is more stable than *ortho* under stress-bearing condition at low temperatures (Coe, 1970; Coe and Kirby, 1975) However, it can be also thought that the stress can be escaped easily from the thin foils (Yagi, private communication) Effect of the thermal stress is uncertain at the present time.

4.2 $P2_1/c$-$C2/c$ phase transformation

(1) Characteristics of the phase transformation

Characteristics of the P-C phase transformation in clinoenstatite observed in the present HTTEM study are summarized as follows:

(a) reversible transformation : The phase transformation occurred reversibly with no appearance of other phases, such as *ortho* or *proto*.

(b) diffusionless transformation : Both the P-C phase transformation in the synthetic and the natural specimens occurred in the same process. Because Fe and Ca ions are not contained in pure enstatite, the P-C phase transformation of the synthetic specimen is apparently not related to the Fe-Mg or Ca diffusion. As for the phase transformation of the natural specimen, a mean free path derived from the diffusion coefficient for the Fe-Mg interdiffusion in pyroxene at 1200°C ($D \sim 10^{-13}$ by extrapolating the data in Figure 12 of Tsuchiyama, 1985) is approximately 0.1 μm/hour. This estimated value is too small to effectuate the growth of the lamellae in the herringbone-like textures observed in the present study. Therefore, the phase transformation of the natural specimen as well as the case of the synthetic one is concluded not to depend on the diffusion.

(c) coexistent stage during the transformation : At the intermediate stage of the phase transformation, the coexistence of both *clino(P)* and *clino(C)* in the herringbone-like texture with the sharp *P/C* interfaces was observed. The coexistence of both phases was observed in a wide temperature range. *Clino(P)* and *clino(C)* have a certain crystallographic orientational relation. The *P/C* interface is coherent and approximately parallel to $(30\bar{1})$ These characteristics of the *P/C* interface are explained by a coherent elastic model of Willaime and Brown (1974) This energy calculation as shown in Figure 30 was carried out by quoting the lattice parameter data at high temperatures from Smyth (1974b) and the elastic constants of augite by Aleksandrov *et al* (1964)

(d) athermal transformation : At the *P-C* coexistent stage for both the synthetic and the natural specimens, one type of lamellae of either *clino(P)* or *clino(C)* became thicker as the other type of lamellae became thinner within a few tens of seconds after temperature changes, irrespective of the heating or cooling process. And then, the thickness of both types of the lamellae became stagnant at constant temperatures. The extent of the reaction depends on the changes in temperature but does not increase with time In fact, the reaction did not proceed in the herringbone-like texture at a constant temperature (1100°C) even for about 5 hours (Figure 15) Therefore, the process of the phase transformation is concluded to be athermal.

(e) small or negative thermal hysteresis: The thermal hysteresis of the phase transformation ($\Delta = A_s - M_s$; see Appendix) is commonly positive and sometimes large However, the thermal hysteresis shown in Table I reveals to be quite small or even negative in the first heat treatment of each specimen. Especially, the thermal hysteresis becomes apparent negative in the subsequent heat treatment, such as the fourth heat treatment (Figure 17b) of the same natural specimen (see Table 1)

(f) nucleation and growth process : In the reheating experiments of the natural specimen, the preferential growth of *clino(C)* from the APB's was observed. To be exact, the nucleation process could not be observed directly However, the APB is naturally expected to act as a nucleus of *clino(C)* because the APB is thought to have locally *C2/c* structure (Morimoto and Tokonami, 1969) and be the good nucleation site of augite (*C2/c*) (Carpenter, 1978) Therefore, the growth process of the *clino(C)* is considered to occur from the APB's as the nucleation sites.

(g) no plastic deformation : Because the *P/C* interface is quite coherent, any defects due to plastic deformation (*e.g.* slip, dislocation) were not observed in either *clino(P)* or *clino(C)* at the coexistence stage.

All of the characteristics (a) to (g) are almost applicable to the case of pigeonite as they are. although

the existence of Ca ions may be some effects on the phase transformation, especially on the *P/C* interfaces (c) In fact, at the coexistent stage of low- and high- pigeonites, the *P/C* interfaces have a sigmoidal shape, not straight as the case of clinoenstatite. It suggests that the orientation of the *P/C* interface, as well as the APB orientation as shown by Carpenter (1978), is affected by the gradient of Ca content in the pigeonite lamellae or the strain field associated with the coarse '001' augite lamellae.

The obvious negative thermal hysteresis in the second heat treatment (Figure 29b) and the growth process of *clino(C)* from the APB's indicate that the *P-C* phase transformation of pigeonite is the same nature of that of the clinoenstatite. Therefore, in the following discussions, clinoenstatite and pigeonite will be treated equally as the *P-C* phase transformation in clinopyroxenes.

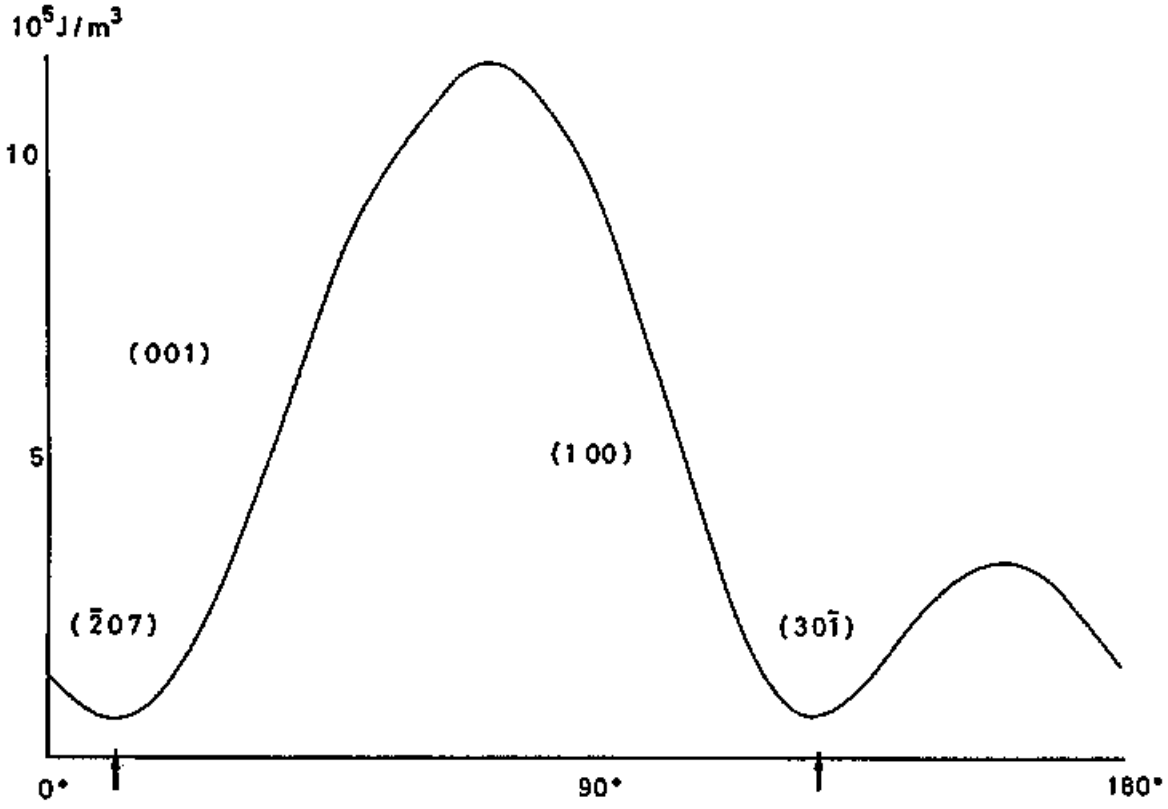

Figure 30. The energy diagram calculated by a coherent elastic model of Willaime and Brown (1974). The calculation is performed by using the lattice parameter data at high temperatures from Smyth (1974b) and the elastic constants by Aleksandrov *et al.* (1964) In this diagram, the elastic energy values for the *P/C* interfaces are plotted against the angle-shifts from the a^* direction. There are two energy minima, indicated by arrows, in this diagram. One of them corresponds to (30$\bar{1}$) which is consistent with the orientation of the *P/C* interfaces observed in this HTTEM study

(2) The nature of the phase transformation

The most fundamental nature of the phase transformation is its order. The order of the *P–C* phase transformation was first proposed to be of a first-order by the X-ray single crystal method (Smyth, 1974b) The present observations of (1) the nucleation & growth process, (2) the coexistence of *clino(P)* and *clino(C)* at the intermediate stage of the transformation, and (3) the existence of the *P/C* interface, are concordant with the first-order transformation.

In addition to the first-order nature of this *P–C* phase transformation, the characteristics (a) to (d) in the previous section [4.2 (1)] display that the *P–C* phase transformations of clinoenstatite and pigeonite occur martensitically In this discussion, martensitic transformation can be defined as "a structural change with a certain crystallographic orientation relation between the parent and the product phases generated by atomic cooperative displacements and not achieved by diffusion" (see Appendix in detail)

The martensitic transformation is generally known as a typical of a first-order. The martensitic transformation was originally found in quenched steels, and since then has been known in other inorganic materials, such as alloys, metals and ceramics. The martensitic transformation has also been reported in minerals, *e.g* the tetragonal-

monoclinic phase transformation in baddelyite (ZrO_2) (Wolten, 1963) and the *proto-clino* phase transformation in enstatite (Smyth, 1974a)

(3) Thermoelastic behaviours

In martensitic transformation, the thermal hysteresis is generally large (*e.g.*, more than 400°C in Fe-Ni alloy) The martensitic transformation generally occurs with extremely high velocities, *e.g* , sometimes as high as the velocity of sound. Therefore, once the martensite generates at its full size, no further growth (or shrinkage) will be observed. In the martensite plates, a number of defects due to plastic deformation are generally included owing to the achievement of the lattice correspondence at the interface.

The remaining characteristics (e) to (g) in the previous section [4 1 (1)], however, are inconsistent with the general features of the martensitic transformation as mentioned above The results of the reheating experiments (*e.g.*, the fourth heat treatment of the natural clinoenstatite in Figure 17b or the second heat treatment of the pigeonite in Figure 29b) revealed that these phase transformations are typical of Class II thermoelastic martensitic transformation. In fact, Figures 17 and 29 resemble closely to Figure 31 by quoting from Fig 2(a) of Hummel and Koger (1967) Figure 31 shows the percent-transformation curves of the thermoelastic martensitic transformation in β_1-brass. Therefore, the HTTEM observation in the present study suggests that the *P-C* phase transformation in clinopyroxenes is the thermoelastic type of the martensitic transformation rather than the normal

(non-thermoelastic) type.

In the thermoelastic transformation, the elastic energy is stored during the forward transformation: the *clino(C)*-to-*clino(P)* phase transformation in this case. This accumulated strain energy, δ (ΔG_{nc}'), assists the reverse transformation: the *clino(P)*-to-*clino(C)* phase transformation in this case. The probable progress in thermoelasticity in the subsequent heat treatment as illustrated in Figures 19 and 29 should be caused by an increase of the stored strain energy during the *clino(C)*-to-*clino(P)* phase transformation.

This thermoelastic martensitic transformation has been studied extensively in the metallurgy and material science, because of its correlation with the unusual mechanical behaviours (see Appendix).

In comparison with the transformation hysteresis loops of the first heating experiments and the reheating experiments for both clinoenstatite (Figure 19) and pigeonite (Figure 29), the "progress in thermoelasticity" seems to occur, *i.e.* the thermal hystereses (Δ's) become smaller with the repetition of the heating experiments. In the field of metallurgy, Dunne and Wayman (1973a, 1973b) demonstrated that the ordering in Fe_3Pt alloy resulted in a progressive change from the normal martensitic transformation to the thermoelastic one; *i e.* thermal hysteresis is positive ($\Delta = A_s - M_s = 365$ °C) in disordered

Fe_3Pt, while thermal hysteresis is negative ($\Delta = A_s - M_s = -35$ °C) in ordered Fe_3Pt This phenomenon has been explained thermodynamically by Tong and Wayman (1975) using a quasi-chemical approach. They illustrated that the To temperature in an AB type alloy decreases in a regular fashion with the long range order parameter (S) coming up to S=1 (full ordered)

The reasons why the progress in thermoelasticity occurs in the subsequent heat treatments in the present study are thought as three following possible interpretations although not well understood; (1) because the ordering of Mg and Fe may be advanced due to the Mg-Fe site exchange but not by diffusion during further heating at high temperatures, as demonstrated in metallurgy, (2) because the foil specimen used in the HTTEM study may obstruct the shape change and thus the stored strain energy by quenching in a foil shape may be larger than the case of the bulk shape as the natural specimen, or (3) because the polysynthetic twins in clinoenstatite and the coarse augite lamellae in pigeonite may obstruct the relaxation of the elastic energy and the stored stain energy may increase in the subsequent experiments.

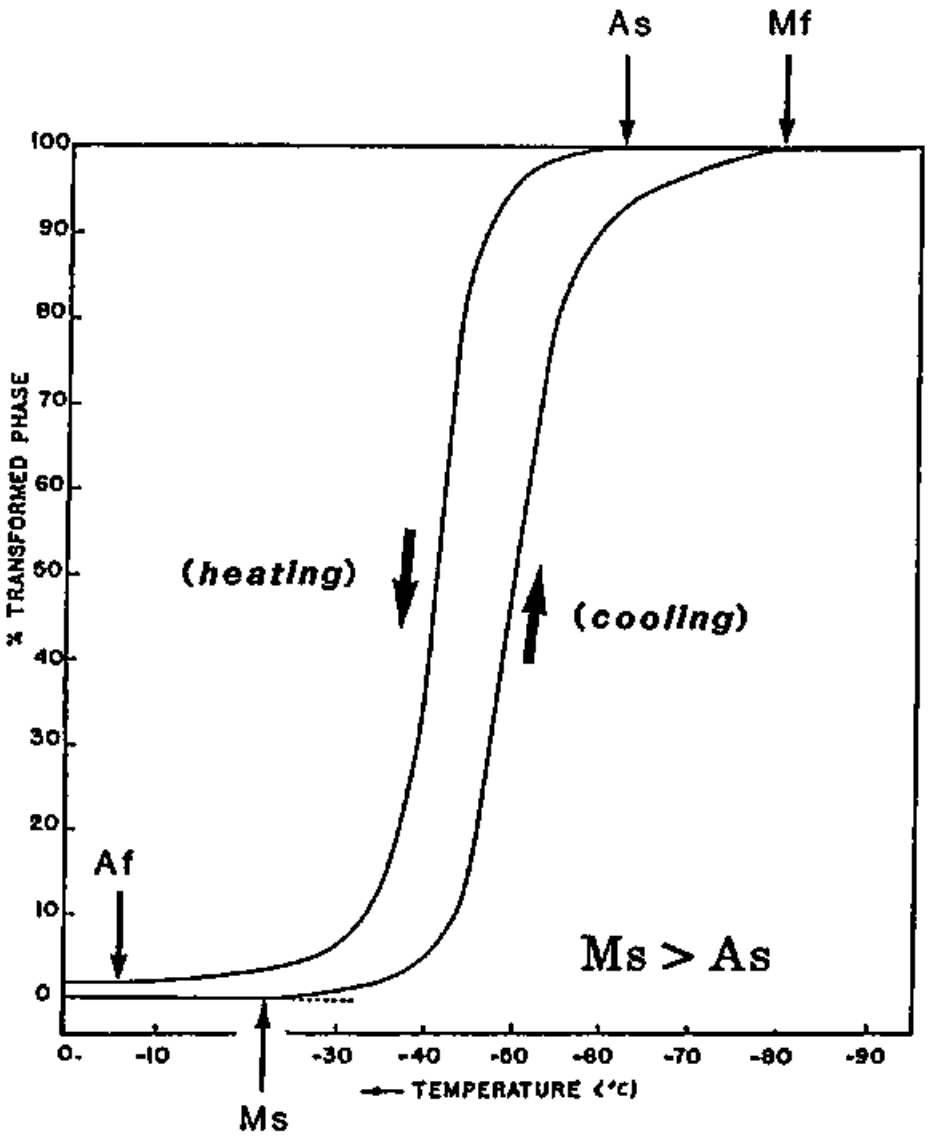

Figure 31. Percent-transformation curves as calculated from the electric resistivity of β_1-brass vs. temperature (after Hummel and Koger, 1967). Both the transformation regions (see Appendix) on the heating and on the cooling are overlapped, and the inequality $M_s > A_s$ holds. This phase transformation is one of the typical instances of Class II thermoelastic martensitic transformation.

(4) Transformation temperatures

Four characteristic temperatures (M_s, M_f, A_s and A_f; see Figure App.-1) of each clinopyroxene are first obtained in the present HTTEM study There are two equilibrium temperatures, T_o and T_o', in thermoelastic transformation (see Appendix) Among them, T_o temperature is adequate as the transformation temperature in the present work because T_o is not affected by the non-chemical behaviours. Four characteristic temperatures and T_o temperatures derived from the equation $T_o = (M_s + A_f)/2$ by Tong and Wayman (1974) are listed in Table 1 Figure 32 is quoted from Fig 2 of Prewitt *et al.* (1971) with three additional T_o data points (asterisks) from the present HTTEM study. This figure shows the variation of "transition" temperature vs. specimen compositions, where open circles represent Apollo 12 pigeonites and open squares represent non-lunar clinopyroxenes. All of these points were determined by the high temperature X-ray diffraction technique only from a gradual weakening and disappearance of the class (*b*) reflections on the heating regardless of the hysteresis effect. Consequently, the temperature assigned to the "transition" depends on the sensitivity of the used equipment to detect weak reflections, as pointed out by Prewitt *et al.* (1971) by themselves. Moreover, their "transition" temperatures only correspond to A_f temperatures. Therefore, the data plotted in Fig 2 of

Prewitt *et al* (1971) are not enough to be thermodynamically treated as the transformation temperatures. For this reason, there are not much points in comparing the present results with other "transition" temperatures in Figure 32 It is clear, however, that the present results on the transformation temperature are not seriously inconsistent with the previous works, although the present *To* temperatures show about 100~200°C higher than the previous "transition" temperatures.

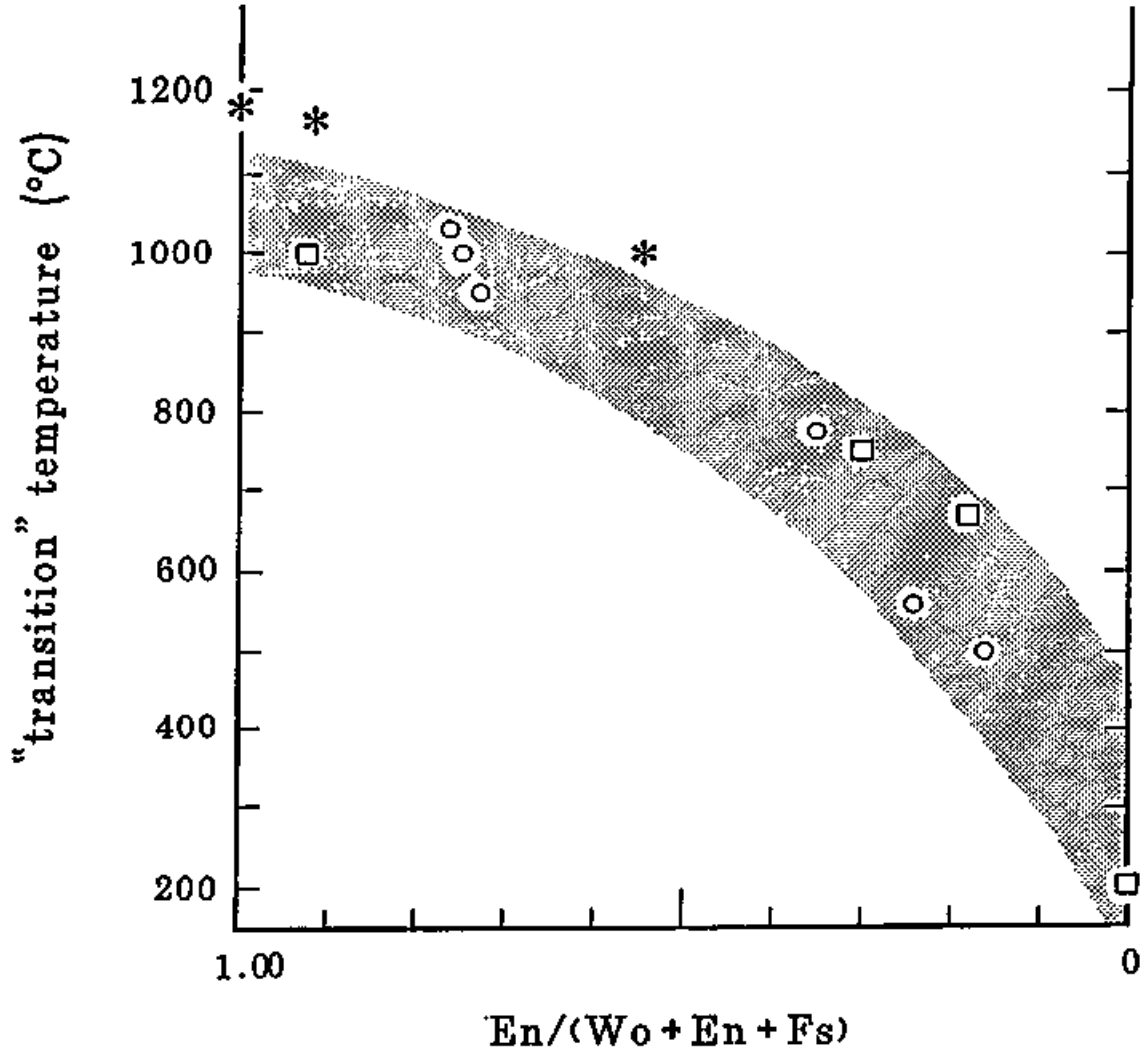

Figure 32. Variation of "transition" temperature vs. composition for several clinopyroxenes. Open circles and squares represent the data from lunar-pigeonites and terrestrial clinopyroxenes, respectively. The shaded region indicates the uncertainty in determining the "transition" temperatures (after Prewitt *et al.*, 1971). Three data (asterisks) derived from the present HTTEM studies are also added to the diagram. The present data implies the real transformation temperatures, *To* (see text)

4 3 Antiphase domain structure

The antiphase domain (APD) structure is a typical resulting microstructure during the *clino(C)*-to-*clino(P)* phase transformation. In the *C*2/*c* structure, all of the silicate chains are symmetrically equivalent. However, there are two symmetrically different silicate chains (designated as the A and B chains) in the $P2_1/c$ structure. During the transformation, the misarrangement in the distribution of the A and B chains generally takes place. As the result, the APD structure, composed of regions with the $P2_1/c$ structure related to each other across antiphase boundaries (APB's) by a translation of $1/2(a+b)$, can be produced. The existence of this APD structure was first suggested by Morimoto and Tokonami (1969) from the diffuseness of the class (*b*) reflections ($h+k$; odd) in volcanic pigeonites. These domains were observed using TEM in lunar or terrestrial pigeonites by Bailey *et al.* (1970), Christie *et al.* (1971) and Champness and Lorimer (1971) On the contrary, the APD's structure has not been reported in clinoenstatite because the clinoenstatites used in the previous works (*e.g* Yasuda *et al* , 1983) would be transformed from *proto* or *ortho*, not from *clino(C)*. The APB's were indeed observed in the natural specimen after the heat treatment in the present HTTEM study The reason why the APB's could not be found in the synthetic clinoenstatite

even after transforming from *clino(C)* is thought that the APB's might migrate and be lost during the cooling in the absence of Ca ions which stabilize them as pointed out by Morimoto and Tokomani (1969)

Carpenter (1978) studied on the APB's in slow-cooled pigeonites in detail and classified into two types; *i e.* APB's cutting the *c* axis (H type) and APB's parallel to the *c* axis (L type) The former have a sigmoidal shape and are approximately parallel to (211) and ($\bar{2}$11), and the latter are straight and approximately parallel to (120) Carpenter (1978) showed using simple structural models that the former provide more suitable sites for Ca^{2+} ions than the latter The L APB's can migrate faster than the H APB's, which would experience a drag effect due to the slowness of Ca diffusion, analogous to the impurity-drag effect on grain boundary motion in metals (Cahn, 1962)

In the present study, the formation of the APD structures in pigeonite was *in situ* observed for the first time using the HTTEM. The formation process of the APD structures in silicate minerals has been *in situ* observed by TEM using the heating stages; for example, in anorthite by Van Tendloo *et al.* (1989) at about 240°C and in kanoite, Ca-poor clinopyroxene in the Ca-Mg-Mn system, by Gordon *et al.* (1981) at about 330°C. In both cases, all of the APB orientations, shapes and positions were essentially unchanged before and after heating through the transformation temperatures. It indicates the stabilization

of APB's by the concentration of Ca or by some defect at the APB's (Gordon *et al.*, 1981) On the contrary, the present results show the remarkable changes in the APB orientations and shapes before and after the first heat treatment. The APB orientations changed from oblique to the *c* axis into parallel to the *c* axis, as pointed out by Fujino *et al.* (1988) The reason why the change in APB orientations took place should be thought that the L APB's became to be in majority against the H ones and consequently the APB's orientations changed seemingly on the whole, not that each APB itself changed its orientation. Therefore, it seems to be doubtful to use the APB orientations as a cooling ratemeter as proposed by Fujino *et al* (1988)

The present HTTEM observations reveal that the *P-C* phase transformation is athermal and then has a transformation region, and that the L APB's form at the earlier stage and the H APB's at the final stage of the *clino(C)*-to-*clino(P)* phase transformation (Figure 24) From the present observations and the structural analysis of the APB's by Carpenter (1978), it is strongly suggested that the L APB's are original APB's of pigeonite while the H APB's are the traces of the *P/C* interfaces. As Carpenter (1978) pointed out, the H APB's which behave as high energy dislocations cutting the SiO_3 silicate chains would migrate and be lost during cooling in the absence of the Ca enrichment onto them. On cooling rapidly, pigeonites cannot remain at high temperatures long enough for the Ca ions to

diffuse onto the H APB's. Consequently, the H APB's may migrate rapidly and be lost while the L APB's may be preserved. On cooling very slowly, on the other hand, the H APB's may be stabilized by the Ca enrichment due to the diffusion, while the L APB's may migrate and be lost during the transformation region. Above hypothesis is concordant with the results of the annealing experiments by Fujino *et al* (1988) and the present study, qualitatively.

5. Conclusions

(1) By use of a newly constructed heating stage, temperatures up to about 1300°C were stably obtained under the HTTEM for more than 1 hour. The present HTTEM system has been proved to be effective to the studies on the phase transformations in pyroxenes, although the vaporization of some specimens is inevitable under such a high temperature and high vacuum conditions.

(2) Both *ortho* and *clino(P)* of enstatite did not transform to *proto*, but to *clino(C)* under the HTTEM. The *ortho*-to-*clino(C)* transformation of enstatite was found for the first time. The reasons why the phase transformation to *proto* did not occur are thought as (a) a deficiency of the heating duration or (b) an effect of the thermal stress caused by the specimen shape (thin foil)

(3) The *P-C* phase transformations in clinoenstatite and pigeonite were successfully observed *in situ* at high temperatures under the HTTEM for the first time. The *P-C* phase transformation reveals to be of a first-order as pointed out by Smyth (1974b), because the coexistence of both phases separeted by the sharp *P/C* interfaces was observed at an intermediate stage of transformation.

(4) Characteristics of the *P-C* phase transformations reveal that the transformations of clinoenstatite and pigeonite occur athermal martensitically and even thermoelastically. This type of transformation has not been

reported in mineralogy and it is the first report of the thermoelastic transformation in minerals.

(5) The formation process of the APD structure in pigeonite was *in situ* observed for the first time using the HTTEM. The HTTEM observations show that the APB's parallel to the *c* axis (L type) form at the earlier stage and the APB's cutting the *c* axis (H type) form at the final stage of the *clino(C)*-to-*clino(P)* transformation on the cooling. H APB's is the traces of the *P/C* interfaces The following hypothesis is proposed. On rapid cooling, the H APB's tend to be lost and the L APB's would be in majority; while on cooling quite slowly, the L APB's tend to migrate away during transformation and the H APB's would be in majority. According to this hypothesis, the fact that the L APB's are commonly found in the quenched pigeonite while the H APB's are commonly observed in the slowly cooled pigeonite, is given a qualitative explanation.

Acknowledgements

The author would like to express his sincere thanks to Dr. Masao Kitamura of Kyoto University for his numerous discussions and helpful comments throughout this study and critical readings of this manuscript.

The author is deeply indebted to Professor Nobuo Morimoto of Osaka Sangyo University for his valuable suggestions and helpful discussions, and to Drs. Akira Tsuchiyama and Seiko Watanabe of Kyoto University, for their discussions and assistance in operation of the HTTEM.

The author is grateful to Professor Katsumichi Yagi of Tokyo Institute of Technology, Professor Kazumi Nishioka of Tokushima University, and Drs. Katsutoshi Tomita and Osamu Tamada of Kyoto University for their helpful comments and discussions.

The author is grateful to Mr. Keiji Shinoda of Osaka City University, Messrs Takashi Fujita, Naoya Imae and Yasuhiro Okamoto of Kyoto University for their technical helps.

References

Aleksandrov, K.S., T V Ryzhova and B.P. Pelikov (1964) The elastic properties of pyroxenes. *Sov Phys. —Crystallogr.*, 8, 589-591.

Bailey, J.C., P.E. Champness, A.C. Dunham, J Esson, W.S. Fyfe. W S. MacKenzie, E.P. Stumpfl and J Zussman (1970) Mineralogy and petrology of Apollo 11 lunar samples. *Proc. Apollo 11 Lunar Sci. Conf.*, 169-194

Bansal, G.K. and A.H. Heuer (1972) On a martensitic transformation in zirconia (ZrO_2) - I Metallographic evidence. *Acta Met.*, 20, 1281.

Bansal, G.K. and A.H. Heuer (1974) On a martensitic transformation in zirconia (ZrO_2) - II Crystallographic aspects. *Acta Met.*, 22, 409-417.

Buseck, P.R., G.L. Nord, Jr and D.R. Veblen (1980) Subsolidus phenomena in pyroxenes. In C.T Prewitt, Ed., Pyroxenes, Mineralogical Society of America: Reviews in Mineralogy, 7, 117-211

Cahn, J.W. (1962) The impurity-drag effect in grain boundary motion. *Acta Met.*, 10, 789-798.

Carpenter, M.A. (1978) Nucleation of augite at antiphase boundaries in pigeonite. *Phys. Chem. Minerals*, 2, 237-251

Carpenter, M.A. (1979) Experimental coarsening of antiphase domains in a silicate mineral *Science*, 206, 681-683.

Champness, P.E. and G.W. Lorimer (1971) An electron

microscopic study of a lunar pyroxene. *Contrib. Mineral Petrol.*, 33, 171-183.

Christie, J.M., J.S Lally, A.H. Heuer, R.M. Fisher, D.T Griggs and S.V Radcliffe (1971) Comparative electron petrography of Apollo 11, Apollo 12, and terrestrial rocks. *Proc. Lunar Sci Conf.*, 2nd, 69-90.

Coe, R.S. (1970) The thermodynamic effect of shear stress on the ortho-clino inversion in enstatite, and other coherent phase transitions characterized by finite simple shear *Contrib. Mineral. Petrol* , 26, 247-264

Coe, R.S. and S.H. Kirby (1975) The orthoenstatite to clinoenstatite transformation by shearing and reversion by annealing: mechanism and potential applications. *Contrib. Mineral Petrol.*, 52, 29-56

Dolino, G., J.P. (1986) The incommensurate phase of quartz In R. Blinc and A.P Levanyuk Eds., *Incommensurate phases in dielectrics* 2, 205-232, Elsevier Science Publishers B.V

Dunne, D.P. and C.M. Wayman (1973a) The effect of austenite ordering on the martensite transformation in Fe-Pt alloys near the composition Fe3Pt: I Morphology and transformation characteristics *Met. Trans.*, 4, 137-145.

Dunne, D.P. and C.M. Wayman (1973b) The effect of austenite ordering on the martensite transformation in Fe-Pt alloys near the composition Fe3Pt: II Crystallography and general features. *Met. Trans.*, 4, 147-152

Feuer, H., L. Schröpfer and H. Fuess (1986) Exsolution and phase transition in pyroxenes (abstr.) *International Mineralogical Association Abstracts with program, 14th General Meeting*, Stanford, 99

Fujino, K., K. Furo and H. Momoi (1988) Preferred orientation of antiphase boundaries in pigeonite as a cooling ratemeter. *Phys. Chem. Minerals*, 15, 329-335

Ghose, S , G Ng and L.S. Walter (1972) Clinopyroxenes from Apollo 12 and 14: exsolution, domain structure and cation order. *Proc. Lunar Sci Conf.*, 3rd, 507-531.

Gordon, W.A., D.R. Peacor, P.E. Brown and E.J Essene (1981) Exsolution relationships in a clinopyroxene of average composition $Ca_{0.43}Mn_{0.69}Mg_{0.82}Si_2O_6$: X-ray diffraction and analytical electron microscopy. *Am. Mineral* , 66, 127-141.

Grove, T.L. (1979) An experimental calibration of submicroscopic textures in lunar pyroxenes: a transmission electron microscope study *Lunar Planet. Sci.*, X, 467-469 (not seen; extracted from Fujino *et al.*, 1988)

Grover, J.E. (1972) The stability of low-clinoenstatite in the system $Mg_2Si_2O_6$-$CaMgSi_2O_6$ (abstr.) *Trans. Am. Geophys. Union, EOS*, 53, 539

Henderson-Brown, M., M.S. Loveday, K.F Hale and T.B. Gibbons (1972) Side entry soft straining and heating stages for *in situ* dynamic experimentsin the IMV electron microscope. *Proc. 5th Europ. Congress on*

Electron Microscopy, Manchester, 328-329 (not seen; extracted from Tighe, 1976)

Hummel, R.E. and J W. Koger (1967) On the characteristic temperatures of the martensitic transformation in β_1 copper-zinc. *Trans. Metal Soc. AIME*, 239, 1655-1656

Kaufman, L. and M. Cohen (1958) Thermodynamics and kinetics of martensitic transformations. In B. Chalmers and R. King Eds., Progress in Metal Physics, 7, 165-245. Pergamon Press, London.

Kirby, S.H. and R.S Coe (1974) The role of crystal defects in the enstatite inversion (abstr.). *Trans. Am. Geophys. Union, EOS*, 55, 419

Komatsu, M (1980) Clinoenstatite in volcanic rocks from the Bonin Islands. *Contrib. Mineral. Petrol.*, 74, 329-338.

Kuno, H (1936) Petrological notes on some pyroxene-andesites from Hakone volcano, with special reference to some types with pigeonite phenocrysts. *Jpn. J. Geol Geogr.*, 13, 107-140

Lally, J.S., A.H. Heuer, G.L. Nord, Jr and J.M. Christie (1975) Subsolidus reactions in lunar pyroxenes: an electron petrographic study *Contrib. Mineral. Petrol* , 51, 263-282

McPartland, J.O. (1962) A high temperature stage for transmission electron microscopy. *Proc. 5th Int. Congress for Electron Microscopy*, Philadelphia, 1, E3-4 (not seen; extracted from Tighe, 1976)

Morimoto. N. and M. Kitamura (1982) Application of 200kV

analytical electron microscopy to the study of fine textures of minerals. *Bull. Mineral* , 104, 241-245

Morimoto, N., N Shimobayashi, A. Tsuchiyama and M. Kitamura (1989) A new heating stage for transmission electron microscopy up to 1300°C. *Mineral. J* , 14, 246-254.

Morimoto, N. and M. Tokonami (1969) Domain structure of pigeonite and clinoenstatite *Am. Mineral.*, 54, 725-740.

Murakami, T , Y Takeuchi and T Yamanaka (1982) The transition of orthoenstatite to protoenstatite and the structure at 1080°C. *Z. Kristallogr.*, 160. 299-312.

Mysen, B.O. and I Kushiro (1988) Condensation, evaporation, melting, and crystallization in the primitive solar nebula: Experimental data in the system $MgO-SiO_2-H_2$ to 1.0×10^{-9} bar and 1870°C with variable oxygen fugacity. *Am. Mineral* , 73, 1-19.

Ozima, M. (1982) Growth of orthoenstatite crystals by the flux method. *J Jap. Assoc. Mineral Petrol. Econ. Geol* , Spec. Issue No. 3, 97-103 (in Japanese)

Perrotta, A.J and D.A. Stephenson (1965) Clinoenstatite: High-low inversion. *Science*, 148, 1090-1091

Prewitt, C.T , J.J Papike and A.E. Bence (1970) Apollo 12 clinopyroxenes: Crystal chemistry and phase transitions (abstr.) *Trans. Am. Geophys. Union, EOS*, 51, 585

Prewitt, C.T , G.E. Brown and J.J Papike (1971) Apollo 12 clinopyroxenes: High temperature X-ray diffraction studies. *Proc. Lunar Sci. Conf* , 2nd, 59-68

Reid, A.M. and A.J Cohen (1967) Some characteristics of enstatite from enstatite achondrites. *Geochim. Cosmochim. Acta*, 31, 661-672

Sadanaga, R. and F.P. Okamura (1971) On the high-clino phase of enstatite. *Mineral J* , 6, 365-374

Sadanaga, R., F.P. Okamura and H. Takeda (1969) X-ray study of the phase transformations of enstatite. *Mineral. J.*, 6, 110-130.

Shiraki, K., N Kuroda, H. Urano and S. Maruyama (1980) Clinoenstatite in boninites from the Bonin Islands, Japan. *Nature*, 285, 31-32.

Smith, J V (1969a) Crystal structure and stability of the $MgSiO_3$ polymorphs: Physical properties and phase relations of Mg, Fe pyroxenes. Mineralogical Society of America, Spec. Paper 2, 3-29

Smith, J V (1969b) Magnesium pyroxene at high temperature: Inversion in clinoenstatite *Nature*, 222, 256-257

Smyth, J.R. (1969) Orthopyroxene-high-low clinopyroxene inversions. *Earth Planet. Sci Lett.*, 6, 406-407

Smyth, J.R.(1974a) Experimental study on the polymorphism of enstatite. *Am. Mineral* , 59, 345-352.

Smyth, J.R.(1974b) The high temperature crystal chemistry of clinohypersthene. *Am. Mineral* , 59, 1069-1082

Sueno, S and C.T Prewitt (1983) Models for the phase transition between orthoferrosilite and high clinoferrosilite. *Fortschr Miner* , 61, 223-241

Tighe, N.J (1976) Experimental techniques. In H.-R. Wenk,

Ed., *Electron Microscopy in Mineralogy*, 144-171 Springer-Verlag, New York.

Tong, H.C. and C.M. Wayman (1974a) Characteristic temperatures and other properties of thermoelastic martensites. *Acta Met.*, 22, 887-896.

Tong, H.C. and C.M. Wayman (1974b) Some stress-temperature-energy relationships for thermoelastic martensitic transformations. *Scripta Met.*, 8, 93-100.

Tong, H.C. and C.M. Wayman (1975) Thermodynamics of thermoelastic martensitic transformations. *Acta Met.*, 23, 209-215

Tsuchiyama, A. (1985) Partial melting kinetics of plagioclase-diopside pairs. *Contrib. Mineral Petrol* , 91, 12-23.

Turner, F.J , H.C. Heard and D.T Griggs (1960) Experimental deformation of enstatite and accompanying inversion to clinoenstatite. *Rept. 21st Int. Geol Congr.*, Copenhagen, 18, 399-408.

Valde, U. (1972) General consideration in specimen stages. *Proc. 5th Europ. Congress on Electron Microscopy*, Manchester, 317-321 (not seen; extracted from Tighe, 1976)

Van Tendeloo, G., S. Ghose and S. Amelinckx (1989) A dynamical models for the $P\bar{1}$-$I\bar{1}$ phase transition in anorthite. $CaAl_2Si_2O_8$ I Evidence from electron microscopy. *Phys. Chem. Minerals*, 16, 311-319

Wayman, C.M. (1983) Phase transformations, nondiffusive In R.W Cahn and P Haasen, Eds., *Physical Metallurgy* (3rd rev), 1031-1074. Elsevier Science Publishers B.V

Willaime, C. and W.L. Brown (1974) A coherent elastic model for the determination of the orientation of exsolution boundaries: Application to feldspars. *Acta Crystallogr.*, A30, 316-331

Wolten, G.M. (1963) Diffusionless phase transformations in zirconia and hafnia. *J. Am. Ceramic Soc.*, 46, 418-422.

Yasuda, M., M. Kitamura and N. Morimoto (1983) Electron microscopy of clinoenstatite from a boninite and a chondrite *Phys. Chem. Minerals*, 9, 192-196.

Appendix. Martensitic transformation

In this appendant chapter, martensitic transformation, including thermoelastic type of that, will be reviewed by quoting chiefly from Wayman (1983)

In the martensitic transformation, the high-temperature phase is generally denoted by "austenite" or parent phase, and the low-temperature phase by "martensite" or product phase. Strictly speaking, "martensitic transformation" indicates the transformation from austenite to martensite upon cooling. However, the term "martensitic transformation" is generally applied to both the martensitic forward transformation and the reverse (or backward) transformation. As the martensitic transformation occurs in some temperature ranges (transformation regions or transformation ranges), four characteristic temperatures are also considered; the start and finish temperatures for the forward (austenite-to-martensite) transformation are designated as M_s and M_f, and similarly for the reverse (martensite-to-austenite) transformation as A_s and A_f, respectively, as summarized in Figure App.- 1

The name "martensite" was originally used to designate the hard microconstituent found in quenched steels. Since then, materials in addition to steels have been also found to exhibit the same type of solid state phase transformation, known as a *martensitic transformation* ——

sometimes also called a *shear* or *displacive transformation*. Indeed the martensitic transformation has been known in other inorganic materials, such as alloys, metals, and ceramics. The martensitic transformation has been also reported in minerals, *e.g.* the tetragonal-monoclinic phase transformation in baddelyite (ZrO_2) (Wolten, 1963; Bansal and Heuer, 1972, 1974) and the *proto-clino(P)* phase transformation in enstatite (Smyth, 1974a)

The martensitic transformation is a structural change with a certain crystallographic orientation relation between the parent and the product phases generated by atomic cooperative displacements ("military" transfer) and not achieved by diffusion. When a new phase is formed from its parent martensitically, discrete regions of the solid typically transform at a high velocity which is independent of temperature. In most cases the amount of transformation resulting is characteristic of the temperature and does not increase with time.

Crystallographic features between the martensite and the parent phase such as the habit (invariant) plane and orientation relationship are usually not expressible in terms of exact relations involving simple Miller indices. The interface boundary between the martensite and its parent is intimately related to the transformation growth process. Such an interface is highly glissile, and from low-temperature experiments is known not to require thermal

activation for its movement. The interface can be totally coherent or semi-coherent, depending upon the particular material undergoing transformation. Due to the achievement of the lattice correspondence at the interface, the transformation generally involves both a macroscopic shape deformation and a microscopic secondary deformation (inhomogeneous shear) The former is usually taken to be a shear parallel to the habit plane plus a simple (unaxial) tensile or compressive strain perpendicular to the habit plane. Such an *invariant plane strain* is the most general that can occur while still maintaining the invariance of the habit plane, and indicates the transformation occurs by cooperative atom movements. The latter, such as slip or twinning, is usually observed in the martensite at the electron microscope scale. This inhomogeneous shear was introduced in the crystallographic description of martensitic transformations to ensure that the habit plane is macroscopically undistorted. This secondary deformation produces the invariant plane condition at the macroscopic scale and provides a semi-coherent glissile interface between the martensite and the austenite Figure App.- 2 is a schematic representation of the appearance of internally twinned and internally slipped martensite plate.

The martensitic transformation is typical of a first-order transition requiring a large chemical driving force. Since the martensitic transformation is diffusionless, its composition does not vary during the phase transformation.

Therefore, the system may be considered as a single component system. As seen in Figure App.- 3, both phases have the same chemical free energy at equilibrium temperature T_0 The phase transformation occurs when the difference in the chemical free energies between both phases attains to a certain amount (a driving force), and usually requires some supercooling or superheating. As a result, the martensitic transformation starts at M_s ($< T_0$) and reverse transformation at A_s ($> T_0$), and therefore the inequalities $A_s > T_0 > M_s$ should always hold. If superheating is approximately equal to supercooling, the equation $T_0 = (M_s + A_s)/2$ holds. This equation proposed experimentally by Kaufman and Cohen (1958) In general, the thermal hysteresis defined as $\Delta = A_s - M_s$ has a large positive value (*e.g.* it attains to more than 400°C in Fe-Ni alloys)

On the contrary, thermoelastic type of the martensitic transformation is characterized by a small hysteresis. This transformation is reported mainly in alloys of the β-phase (3/2 electron/atom Hume-Rothery phase) type, such as β_1-brass (Hummel and Koger, 1967) Thermoelastic and non-thermoelastic martensitic transformations may be represented by Au-Cd and Fe-Ni alloys, respectively, as indicated in Figure App.- 4 (Kaufman and Cohen, 1958) where it can be seen that a substantial difference in transformation hysteresis exists.

Thermoelastic Martensitic Transformation

In the thermoelastic martensitic transformation, the parent phase accommodation of the martensite plates appears to be essentially elastic, with no dislocation generation, and the interface remains glissile, capable of "backwards" movement and the shrinkage of martensite plates during heating for the reverse transformation. In such thermoelastic transformation, stored elastic energy contributes to the driving force for the reverse transformation.

The free energy change per mole associated with the martensitic transformation, $\Delta G = G^M - G^A$, is generally given by (the superscripts A and M signify austenite and martensite, respectively);

$$\Delta G = \Delta G_c + \Delta G_{nc},$$

where ΔG_c is the chemical free energy change and ΔG_{nc} is the non-chemical free energy opposing the transformation, and the G represents at the forward transformation (*vice versa*; $\Delta G' = G^A - G^M$, at reverse transformation) The term ΔG_c is negative below T_0 and the positive term ΔG_{nc} takes account of changes in energy due to elastic, surface, magnetic or other non-chemical effects. Since the interface is fully coherent in the thermoelastic transformation, the surface energy term should be neglected, and thus the elastic energy term will dominate, increasing rapidly with the martensite plate size. This elastic energy will not be spent by forming the shape deformation or the invariant

plane strain, and will be accumulated. As transformation progresses, the term ΔG_{nc} progressively increases because of the accumulation of the elastic strain energy, and finally reaches its saturation value This accumulated non-chemical free energy term assists the reverse transformation.

According to Tong and Wayman (1974a, 1974b), two equilibrium temperatures, T_0 and T_0' are associated with thermoelastic martensitic transformation. T_0 is the temperature where $\Delta G_c=0$. T_0 is bracketed by M_s and A_f such that $A_f > T_0 > M_s$ If the interval A_f-M_s is small and if the supercooling is approximately equal to superheating, the approximation

$$T_0 = (A_f + M_s)/2$$

holds. On the other hand, T_0' is another characteristic temperature where $\Delta G_o'+\delta(\Delta G_{nc}')=0$, where $\delta(\Delta G_{nc}')$ is a saturation value accumulated during the forward transformation. T_0' is similarly bracketed by A_s and M_f such that $A_s > T_0' > M_f$ Similarly, the approximation

$$T_0' = (A_s + M_f)/2$$

holds. The thermal hysteresis becomes either positive or negative in accordance with the magnitude of the difference between two temperatures, T_0 and T_0' Dunne and Wayman (1973a, 1973b) classified the thermoelastic martensitic transformations into two categories: Class I, where the temperature range M_s to M_f is small and

$$A_f > A_s > M_s > M_f,$$

there are four different ways to locate T_0 and T_0'; and

Class II, where the range between M_s and M_f is large and

$$A_f > T_0 > M_s > A_s > T_0' > M_f$$

(Figure App.- 5)

This type of transformation is also characterized by the continuous growth (or shrinkage) of martensite (or austenite) plates during the transformation. For the normal (non-thermoelastic) type, the transformation proceeds by forming the martensite plates one after the other on cooling. Each plate has been already in its full size at the time of its formation and will not grow further upon subsequent cooling. The amount of transformation depends on the number of the martensite plates. In contrast, for the thermoelastic type, the transformation proceeds by growth of the martensite plates on cooling Growth of martensite plates ceases when cooling is stopped, but resumes further upon subsequent cooling The reverse transformation upon heating instantaneously occurs by the backwards movement of the interface, *i e.* the martensite plates "shrink" In this case, the size of a martensite plate corresponds to a free energy minimum at a given temperature. For example, if the temperature is decreased, ΔG_c decreases, and thus a martensite plate grows until another minimum is reached. On the contrary, if the temperature is raised, ΔG_c increases and the martensite plate shrinks until another minimum is reached. When ΔG for the system takes a minimum under a given set of conditions, the system can be described to be

in a state of thermoelastic equilibrium. This is the origin of the terminology "thermoelastic transformation"

The thermoelastic martensitic transformations are accompanied by very unusual mechanical behaviours, such as the shape memory effect (SME), superelasticity associated with the formation of a reversible stress-induced martensite (SIM), the rubberlike effect, and so on. Therefore, the thermoelastic martensitic transformation has been studied extensively in the metallurgy and material science. However, this type of transformation has not been reported in mineralogy.

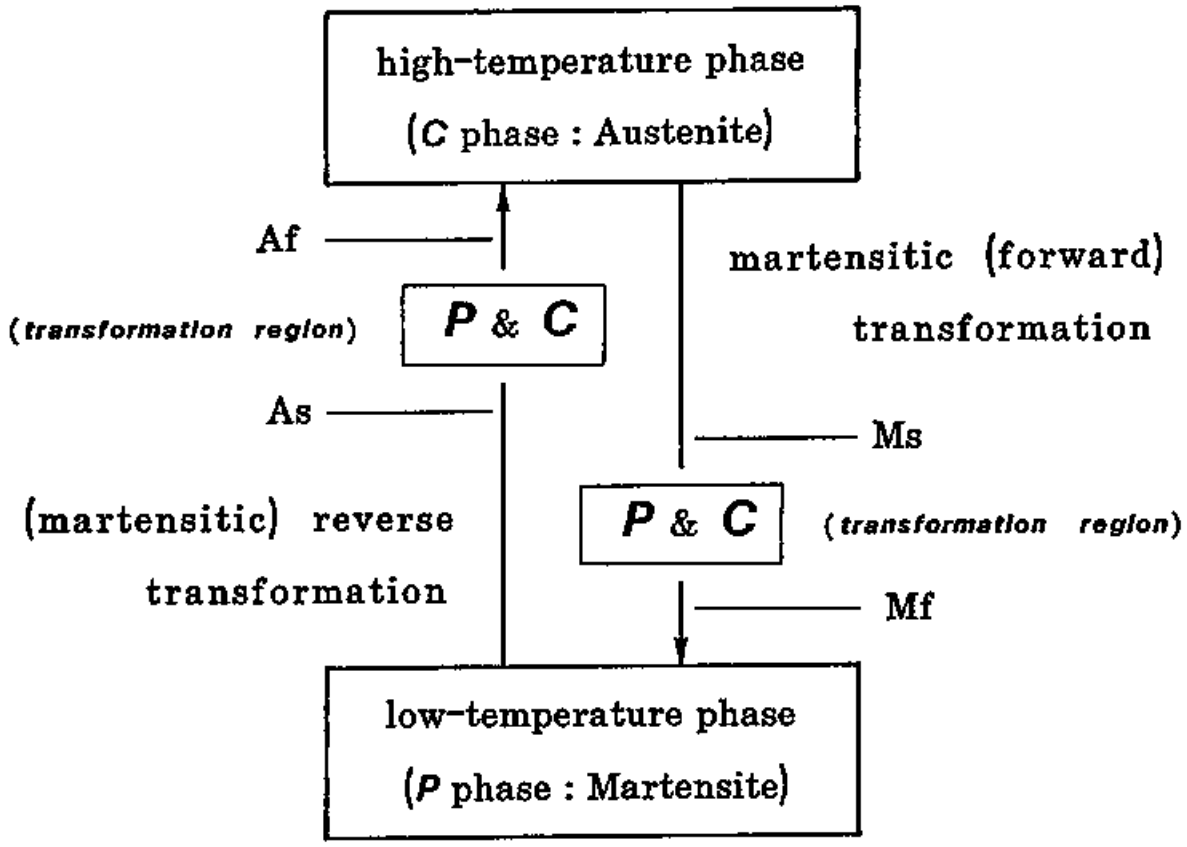

Figure App.-1. Schematic representation of the terms of martensitic transformation. 'P' and 'C' represent $P2_1/c$ and $C2/c$ phases treated in this study, respectively The usual terms 'martensite' and 'austenite' in metallurgy, correspond to $P2_1/c$ and $C2/c$ in this study, respectively. Both $P2_1/c$ and $C2/c$ phases are coexistent in the transformation region (or transformation range). There are four characteristic temperatures: M_s(martensitic start temperature), M_f(martensitic finish temperature), A_s(austenitic start temperature), and A_f(austenitic finish temperature)

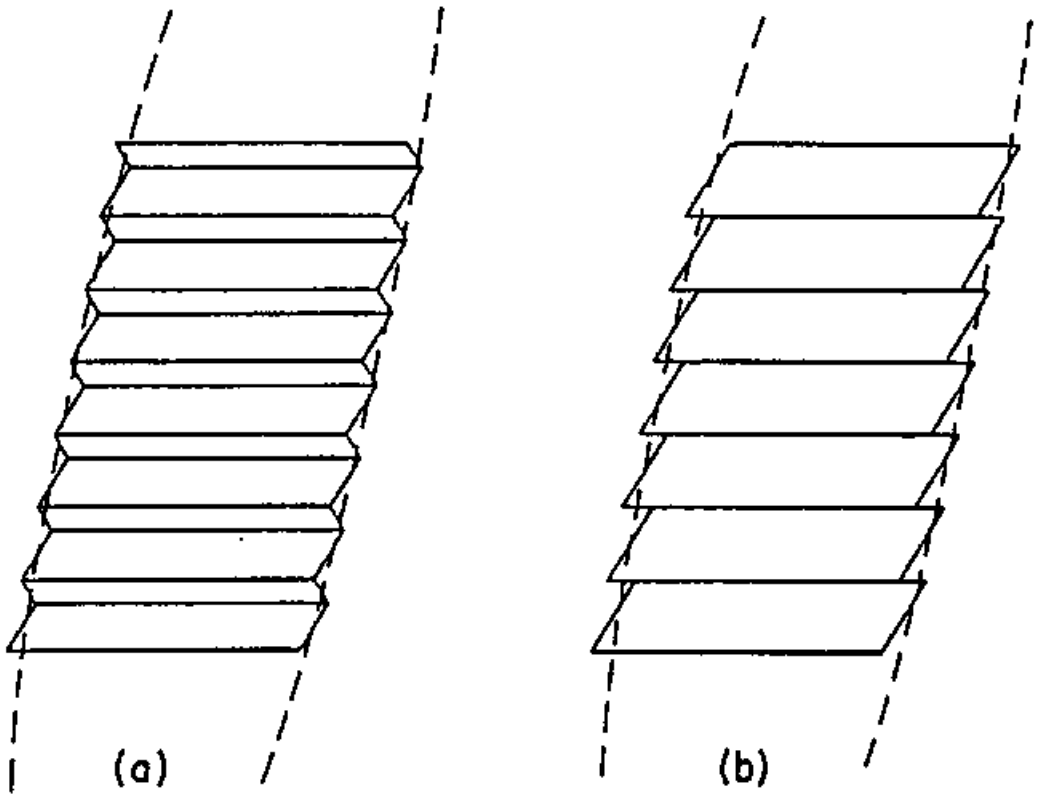

Figure App.-2. Schematic representation of the inhomogeneous shear in a martensitic transformation involving (a) internally twinned, and (b) internally slipped martensite plates (after Wayman, 1983). The interface remains macroscopically undistorted owing to the inhomogeneous deformation.

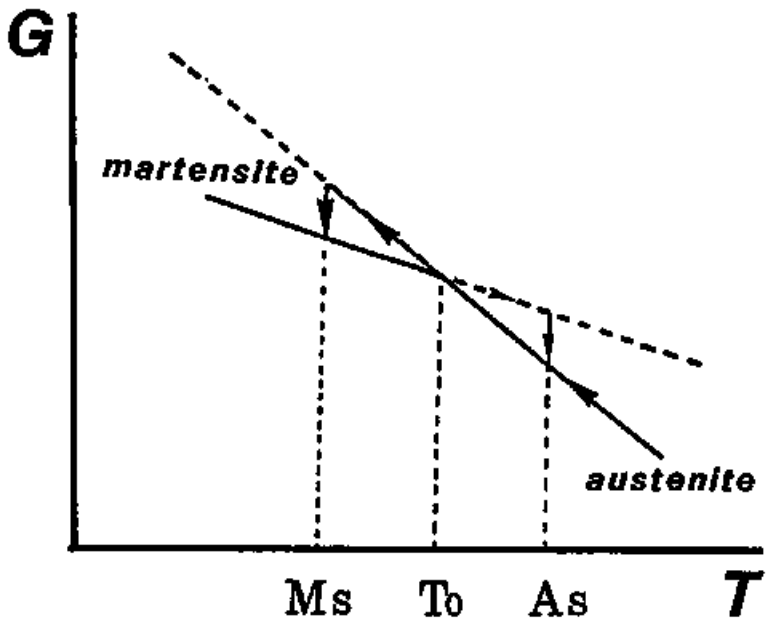

Figure App.-3. Schematic diagram showing the free energy change for a martensitic transformation. At the temperature T = T_0, the chemical free energies of both phases are equal. The forward transformation requires some supercooling and starts at M_s (< T_0) on cooling. The reverse transformation similarly starts at A_s (> T_0) on heating. Kaufman and Cohen (1958) proposed that T_0 can be determined by bracketing it between M_s and A_s, according to

$$T_0 = (M_s + A_s)/2.$$

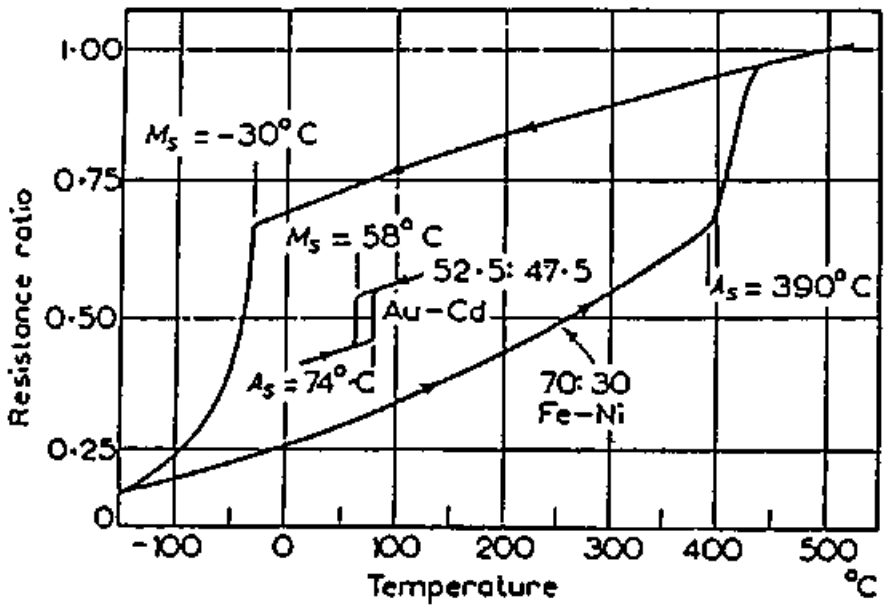

Figure App.-4. Electrical resistivity vs. temperature hysteresis loops for Fe-Ni (non-thermoelastic martensitic transformation) and Au-Cd (thermoelastic martensitic transformation) alloys (after Kaufman and Cohen, 1958).

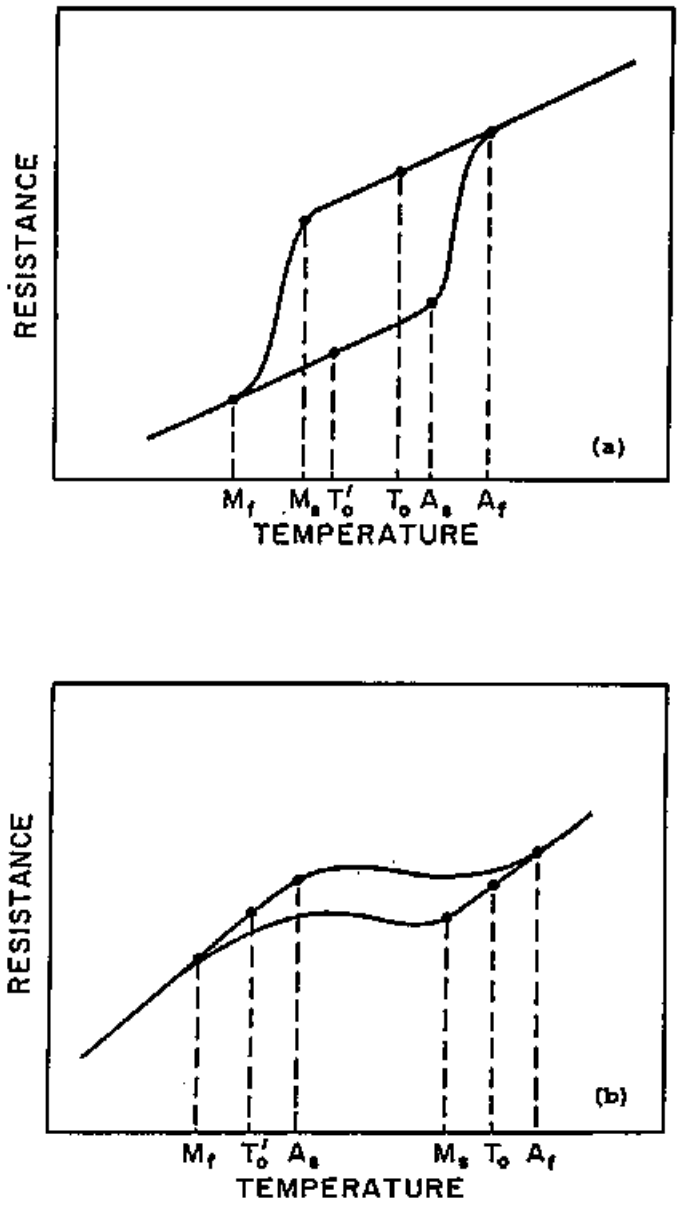

Figure App.-5. Schematic representation of electrical resistivity vs. temperature hysteresis loops for (a) Class I and (b) Class II thermoelastic martensitic transformation. In Class I transformation, the temperature range M_s to M_f is small and the inequality $A_s > M_s$ holds; in Class II transformation, the temperature range M_s to M_f is large and the inequality $A_s < M_s$ holds.